



Norwegian University
of Life Sciences

Master's Thesis 2018 30 ECTS

Faculty of Science and Technology (REALTEK)
Themistoklis Tsalkatidis

Parametric study of an aluminium K-joint

Trym Hauge Nilsen

Civil engineering and architecture
Faculty of Science and Technology (REALTEK)

Preface

This master thesis marks the end of my five years education – Civil engineering and architecture at the Norwegian University of Life Science (NMBU).

The topic of this master thesis was selected in collaboration with associate professor Themistoklis Tsalkatidis, who also was my thesis supervisor. The reason for selecting this topic was my interest in Aluminium and my wish to learn more about a material that has not been of high priority in prior years of my education. I have also good experiences with FEM programming and numerical analyses was a natural way to investigate the selected structure. The work has been time consuming and the learning curve was steep throughout the project. It has given me more experience in FEM programming, especially in software program ANSYS, and I have learned much about aluminium as a material. This experience is something I will bring with me in future years.

I would like to thank my supervisor associate professor Themistoklis Tsalkatidis for his guidance and interest during the writing and modelling of this theses. Especially his positivity and motivation when challenges were encountered.

I would also like to thank my classmates for a good environment to work in. A special thanks to Sonja Helene Servan, Synne Lofthus Rooth and Tord Hauge Nilsen for looking critically through my work and helping me make the thesis better. Finally, I would like to thank my family and friends for encouragement and support during the spring.

Abstract

Aluminium is a construction material which has increased in use over the past 50 years. Its low weight makes it preferable in portable structures. K-joint is the main joint in trusses and these trusses are used in scaffolds and moveable stages where large spans are present. Although some research has been done during the last 20 years, there is still a lot of potential to make more studies of aluminium structures. In this thesis, numerical models of a K-joint made from CHS profiles have been made based on the experimental data in Đuričić et al. (2017). It is parametric studies where brace angle and chord thickness, and their influence on deformation and resistance, have been investigated. Since there is no direct approach described to calculate resistance in aluminium K-joints, it has also been investigated if the steel theory in EN1993-1-8 (2005) sufficiently describes the behaviour of the models created.

Four case studies were modelled in FEM program ANSYS. A reference model with brace angle 45° and chord thickness of 2 mm was made and validated with the experimental results in Đuričić et al. (2017). Two models with brace angle 30° and 60° were created to study the effect of brace angle changes. To investigate the chord thickness, a model where the chord thickness was increased from 2 mm to 3 mm was made. All the models were loaded at the compressed brace member, the resulting deformations and von mises stresses were investigated. Strength of the models is found with the deformation limits described by Lu et al. (1994). The strengths are compared to each other to investigate the influence of the different parameters. Design resistances are calculated based on the steel theory in EN1993-1-8(2005), with the addition of aluminium softening described in EN1999-1-1(2007). These calculations are compared to the numerically obtained strengths, in order to investigate the correlation between them.

The numerical results experience a 20 % increase of the design strength against chord plastification as the brace angle is decreased from 45° to 30° and an increase of 5 % when the angle is changed from 60° to 45° . The model with increased chord thickness experiences a different failure mode than the other models. The braces fail from stresses in the heat affected zones exceeding the ultimate strength.

Hand calculation results show a good correlation with the model with low brace angle. It gives very conservative values for the K-joints with larger brace angles. The K-joint with chord thickness 3 mm is not sufficiently described by the steel theory since axial failure in the braces needs to be considered in addition to the chord plastification failure.

Sammendrag

Bruken av aluminium som et konstruksjonsmateriale har økt over de siste 50 årene. Den lave vekten gjør det foretrukket i midlertidige konstruksjoner. K-forbindelser er hovedkomponenten i fagverk som brukes i stillas og midlertidige scener hvor store spenn er tilstede. Det er gjort noen studier på denne typen forbindelser de siste 20 årene, men det er fortsatt stort potensial til å forske mer på dette. I denne oppgaven er det laget numeriske modeller av K-forbindelser laget av CHS profiler basert på eksperimentelle data i Đuričić et al. (2017). Det er en parametriske studie hvor stegstavens vinkel og tykkelsen på gurtstaven, og deres innvirkning på deformasjon og styrke, har blitt undersøkt. Siden det ikke finnes en direkte metode for å beregne styrke i aluminium K-forbindelser, har det også blitt undersøkt om stålteorien i EN1993-1-8 (2005) beskriver oppførselen til modellene tilstrekkelig.

Fire strukturer har blitt modelert i FEM programmet ANSYS. En referansemodell med stegvinkel på 45° og gurtstavtykkelse på 2 mm har blitt laget og validert opp mot de eksperimentelle resultatene i Đuričić et al. (2017). To modeller med stegvinkel på 30° og 60° er bygget for å studere effekten av endringer av vinkelen. For å undersøke gurttykkelsen ble det modellert en K-forbindelse med økt gurttykkelse fra 2 mm til 3 mm. Alle modellene var lastet på stegstaven som var i trykk, resulterende deformasjoner og von mises spenninger ble undersøkt. Styrken til modellene er funnet med deformasjonsgrensene beskrevet av Lu et al. (1994). Styrkene er sammenlignet for å undersøke påvirkningen av de forskjellige parametrene. Dimensjonerende styrke er beregnet basert på stålteorien i EN1993-1-8 (2005), med innvirkning av oppmykning i aluminium beskrevet i EN1999-1-1 (2007). Disse beregningene er sammenliknet med de numeriske styrkene for å undersøke sammenhengen mellom dem.

De numeriske resultatene opplever en økning av styrken mot flensbrudd i gurten på 20 % når stegvinkelen endres fra 45° til 30° og en økning på 5 % når vinkelen endres fra 60° til 45° . Modellen med økt gurttykkelse opplever en annen bruddform enn de andre modellene. Stegstavene går i brudd fra de aksielle spenningene i de varmpåvirkede sonene som overstiger bruddspenningene.

Håndberegningene gir god korrelasjon med modellen med liten stegvinkel. De gir veldig konservative verdier for K-forbindelsene med større stegvinkler. Forbindelsen med gurttykkelse på 3 mm er ikke tilstrekkelig beskrevet av stålteorien siden aksielt brudd i stegene må vurderes i tillegg til flensbrudd i gurten.

Table of content

Preface	2
Abstract	4
Sammendrag	6
List of figures	12
List of tables	13
List of symbols	14
1 Introduction	16
1.1 Background.....	16
1.2 Objective.....	16
2 Theory	18
2.1 Material	18
2.1.1 History and use of aluminium	18
2.1.2 Numbering and temper designations of aluminium alloys.....	18
2.1.3 Aluminium alloy EN AW-6082 T6.....	20
2.1.4 Heat-affected zone.....	21
2.2 Stress-strain relationship	22
2.3 Design of K-joints	25
2.3.1 Failure modes	25
2.3.2 Design axial resistances for K-joints.....	27
2.3.3 Aluminium softening reduction factor	29
2.4 Previous analysis of k-joints	30
2.5 The finite element method.....	31
2.5.1 Boundary conditions and loading.....	33
2.5.2 Linear analysis.....	33
2.5.3 Nonlinear analysis	33
2.6 ANSYS Mechanical APDL.....	34

2.6.1 Element type used in ANSYS	34
2.6.2 Element size and Meshing.....	35
2.6.3 Multilinear isotropic hardening (TB,MISO)	35
3 Methodology	36
3.1 Introduction	36
3.2 Different K-joints to be modelled	36
3.3 Numerical analysis	37
3.3.1 Geometry	37
3.3.2 Element selection and meshing	38
3.3.3 Material input	39
3.3.4 Stress-strain curves.....	40
3.3.5 Boundary conditions and loads	43
3.3.6 Analysis type and postprocessing	44
3.5 Hand calculations of K-joint	45
3.5.1 Calculations without consideration of heat affected zone.....	45
3.5.2 Calculations with consideration of heat affected zone.....	46
3.5.3 Comparison of numerical results and hand calculations.....	47
4 Results	48
4.1 Numerical analysis	48
4.2 Hand calculations	54
4.3 Comparison of Numerical results and hand calculations	55
5 Discussion	58
5.1 Modelling process	58
5.2 Validation of the model.....	58
5.3 Interpretation of numerical results of parametric study	59
5.3.1 Difference in brace angle	59
5.3.2 Increased thickness of chord member	59

5.4 Comparison of hand calculated results and numerical results	60
5.4.1 Different brace angles	60
5.4.2 Different thickness of chord	61
6 Conclusion.....	62
7 Recommended for future work	64
8 References	66
Annex A	68
Annex B.....	72
Annex C.....	74

List of figures

Figure 1: Bi-linear model (left) and three-linear model (right) of stress-strain relationship (EN1999-1-1, 2007)	24
Figure 2: Failure modes for joints made of CHS-profiles (EN1993-1-8, 2005)	26
Figure 3: Gap K-joint with geometric sizes (EN1993-1-8, 2005).....	27
Figure 4: Logical diagram of the process of finite element analysis(Bathe, 2006).....	32
Figure 5: Geometry of SOLID285 element (ANSYS, version 18.2, Academic).....	35
Figure 6: Geometry of investigated models	37
Figure 7: Initial model of k-joint with angle of 45 degrees.....	38
Figure 8: Mesh of k-joint	39
Figure 9: Plot of Ø50x2 mm stress-strain curve	41
Figure 10: Plot of Ø20x2 mm stress-strain curve	41
Figure 11: Plot of HAZ1 stress-strain curve	42
Figure 12: Plot of HAZ2 stress-strain curve	43
Figure 13: Structure with applied boundary conditions and loading	43
Figure 14: Extent of heat affected zone(Đuričić et al., 2017)	46
Figure 15: Deformed shape of model 1	48
Figure 16: Force-deformation of model 1	48
Figure 17: Contour plot of von mises stress in HAZ1 of model 1	49
Figure 18: Deformed shape of model 2.....	50
Figure 19: Force-deformation of model 2	50
Figure 20: Deformed shape of model 3.....	51
Figure 21: Force-deformation of model 3	51
Figure 22: Deformed shape of model 4.....	52
Figure 23: Plot of force-deformation for model 4.....	52
Figure 24: Contour plot of von mises stress in HAZ1 of model 4.....	53
Figure 25: Combined force-deformation graph for all models	53
Figure 26: Joint resistances for different angled k-joints.....	55

List of tables

Table 1: Numerical designation system for wrought aluminium alloys (Müller, 2011).....	19
Table 2: Basic temper designation (Müller, 2011).....	20
Table 3: Chemical composition of EN AW-6082, in %, rest is aluminium (EN573-3, 2013)	20
Table 4: Mechanical properties of EN AW-6082 T6 (EN755-2, 2016).....	20
Table 5: Engineering stress-strain relations (Đuričić et al., 2017).....	21
Table 6: Stresses of material in HAZs (Heat affected zones) (Đuričić et al., 2017).....	22
Table 7: Validity range for welded joints between CHS brace members and CHS chords (EN1993-1-8, 2005)	27
Table 8: Different models to investigate	36
Table 9: True stresses in CHS profile	39
Table 10: Stresses for heat affected zones	40
Table 11: Multilinear isotropic hardening table for Ø50x2 mm in ANSYS	40
Table 12: Multilinear isotropic hardening table for Ø20x2 mm in ANSYS	41
Table 13: Multilinear isotropic hardening table for HAZ1 in ANSYS	42
Table 14: Multilinear isotropic hardening table for HAZ2 in ANSYS	42
Table 15: Pressure applied on compressed brace	44
Table 16: Calculations according to Eurocode 3 part 1-8	45
Table 17: Calculation of design resistance of softened cross-section	47
Table 18: Results of hand calculations for model 1	54
Table 19: Results of hand calculations for model 2	54
Table 20: Results of hand calculations for model 3	54
Table 21: Results of all hand calculations for model 4	55
Table 22: Relation between numerical results and hand calculations.....	56
Table 23: Relation between different angled connections	56

List of symbols

Δ_u - ultimate strength deformation limit

Δ_s - serviceability strength limit

γ - ratio of brace member diameter to twice its wall thickness

γ_{M5} - partial safety factor for resistance of joints

ε - strain

ε_e - strain corresponding to f_e

ε_{eng} - engineering strain

ε_p - strain corresponding to f_p

ε_{max} - strain corresponding to f_{max}

θ_i - angle between brace member i and chord member

$\rho_{0,haz}$ - strength reduction factor for heat affected zone

σ - stress

σ_{eng} - engineering stress

A - elongation measured over a gauge length of $5.65\sqrt{S_0}$ (where S_0 is the initial cross-sectional area of the test piece)

A_{50mm} - elongation measured over a gauge length of 50 mm

d_i - diameter of brace member i

d_0 - diameter of chord

E - elastic modulus

E_1 - first hardening modulus

E_2 - second hardening modulus

f_0 - 0,2% proof strength

$f_{1\%}$ - 1% tensile strength

$f_{3\%}$ - 3% tensile strength

f_u - ultimate tensile strength

$f_{0,HAZ}$ - 0,2% proof strength of heat affected zone

$f_{u,HAZ}$ - ultimate tensile strength of heat affected zone

f_p - elastic limit of proportionality

f_{max} - maximum stress in stress-strain diagram

f_e - limit of elasticity

f_{y0} - yield strength of chord
 g - gap between brace members
HB - Brinell hardness
HV - Vickers hardness
 \mathbf{K} - stiffness matrix
 k_g - k-joint geometry factor
 k_p - chord stress factor
 k_{al} - aluminium softening reduction factor
 L^* - arc length of softening zone
 L - circumference of chord member cross section
 $N_{i,Rd}$ - resistance force in brace member i
 N_u - ultimate strength
 N_s - serviceability strength
 \mathbf{R} – load vector
 $R_{p0,2}$ - yield stress
 R_m - tensile strength
 t_i - thickness of brace member i
 t_0 - thickness of chord
 \mathbf{U} - displacement vector

1 Introduction

1.1 Background

Aluminium is a light material, this reduces the cost of transportation, work and assembly since less resources are needed to transfer the elements. Another advantage is the ease of recycling aluminium, since only 5% of the energy required for primary production is used for recycling. This can help achieve the norms on sustainability and recyclability in the construction industry, to limit the impact on the environment in the manufacturing and building process. The use of aluminium as a construction material has increased, therefore a Eurocode solely about aluminium was created. Eurocode 9 establishes design criteria for this material (Müller, 2011). There are some disadvantages of aluminium as well. The modulus of elasticity is about one third that of steel, the level of heat conductivity is high and the production cost is high (Đuričić et al., 2017).

K-joints are the main components of truss elements. Trusses are used for large spans and aluminium trusses are often used for stage elements, scaffolds and other transportable structures where the decrease of weight is of importance. They consist of chords and braces welded together and these are mainly loaded by axial compression or tension forces (Đuričić et al., 2017).

Circular hollow sections (CHS) have excellent properties in resisting compression, tension, bending and torsion. Related to other elements, CHS have a favourable shape when being subjected to loading. With these good characteristics, open designs can be made allowing an architecturally attractive shape of elements (Wardenier et al., 2008).

1.2 Objective

Various shapes and sizes of aluminium trusses can create many different brace angles in the K-joints. This is a parametric study of a K-joint made from circular hollow sections (CHS) in aluminium alloy EN AW-6082 T6. The primary objective is to investigate the effect of changing brace angle and thickness of the chord, with focus on how this influences deformation

and resistance of the connection. While K-joints made from steel have been studied extensively, similar joints made from aluminium have been less investigated. The most common approach for designing K-joints of aluminium CHS profiles is to use the same theory as for steel joints. Therefore, a secondary objective of this thesis is to investigate if the embracement of steel related theories sufficiently describes the behaviour of aluminium K-joints, especially their design resistance capacities. This will be investigated numerically by constructing three-dimensional models in ANSYS, a popular finite element program. Previous experiments on CHS K-joints in aluminium have been conducted by Đuričić et al. (2017) and the numerical models are created from the data in these experiments. The results from this study have been used to verify the numerical model.

2 Theory

2.1 Material

Aluminium has a density of approximately 2700 kg/m^3 , about one third of steel. It has a tensile strength of $90\text{-}140 \text{ N/mm}^2$ and is classified as a weak metal. This means that for structural applications the aluminium must be strengthened. Strengthening is done by the method of alloying (Müller, 2011).

2.1.1 History and use of aluminium

Using aluminium alloys in structural engineering is quite new. While aluminium became possible to isolate in 1827, industrial production of aluminium did not start before 1886. Until the second world war, aluminium was only used for specific constructions, such as the aeronautical industry. It was not until after the second world war that the aluminium alloys started to be developed for use in civil engineering. The first building structures that consisted of aluminium alloys appeared as prefabricated systems in the early fifties in central Europe. At that time the absence of recommendations and codifications made the structural design difficult for engineers and controlling bodies. In Europe, this has been overcome first by the ECCS Recommendations issued in 1978 and up until now with the Eurocode 9 “Design of Aluminium Structures.” However, there is still much potential in these materials and further research must be performed (Mazzolani, 2012).

2.1.2 Numbering and temper designations of aluminium alloys

The main alloying elements create a base for numbering and incorporation within designated series. Currently the aluminium alloy designation for wrought aluminium is based on the system for alloy designation administered by the Aluminium Association Inc. The first digit in the alloy numbering relates to the series group, this is associated to the major alloying element used. The different series are presented in Table 1. If the alloys are Heat-treatable (HT) or non-heat-treatable (NHT) they are classified in different types (Müller, 2011).

Table 1: Numerical designation system for wrought aluminium alloys (Müller, 2011)

Series	Alloying elements	Type
1xxx	None (aluminium 99% and greater)	NHT
2xxx	Copper (Cu)	HT
3xxx	Manganese (Mn)	NHT
4xxx	Silicon (Si)	NHT
5xxx	Magnesium (Mg)	NHT
6xxx	Magnesium and silicon (MgSi)	HT
7xxx	Zinc (Zn)	HT
8xxx	Other elements	

If there is a modification from the specific alloy the second digit in the alloy numbering will be different from 0. The last two digits are there to identify the specific alloy in its series (Müller, 2011).

Due to the availability of different tempers, there is an additional mark for the aluminium alloy numbering. This temper designation and the resulting properties are dependent for the types of heat-treatable and non-heat-treatable alloys. For heat-treatable alloys, heat can be used to strengthen or soften the material, and heat is often used to help the forming process. To restore original properties, heat-treatable alloys can be re-heat-treated after the forming process is completed. For non-heat-treatable alloys, properties can only be improved by cold-working (Müller, 2011).

There are five basic designations used in the aluminium alloy temper designation system. For these five groupings the letters F, O, H, W and T is used. These letters represent different heat-treatments. The basic treatments are listed in Table 2 (Müller, 2011).

Table 2: Basic temper designation (Müller, 2011)

Letter	Description	Meaning
F	As fabricated	Forming process with no special control over thermal or strain hardening
O	Annealed	Heat treated to give min. strength improving ductility and dimensionality
H	Strain hardened	Strengthened by cold working
W	Heat treated	Solution heat treated but produces an unstable temper
T	Heat treated	Thermally heat treated with or without additional strain hardening

An additional number can be added to the temper designation to explain what type of treatment the alloy has been exposed to (Müller, 2011).

2.1.3 Aluminium alloy EN AW-6082 T6

The aluminium alloy EN AW-6082 T6 is a high strength alloy used mainly for highly loaded structures. The 6000-series of aluminium alloys is much used for their favourable combination of mechanical properties. Alloy 6082 has a high strength after heat treatment as well as good corrosion resistance and good weldability (Wang et al., 2015). The temper T6 implies that the solution is heat treated, quenched and artificially aged (Müller, 2011). Table 3 and Table 4 gives chemical composition and mechanical properties of aluminium alloy EN AW-6082 T6.

Table 3: Chemical composition of EN AW-6082, in %, rest is aluminium (EN573-3, 2013)

Si	Fe	Cu	Mn	Mg	Cr	Zn	Ti	Others	
								Each	Total
0,7-1,3	0,50	0,10	0,40-1,0	0,6-1,2	0,25	0,20	0,15	0,05	0,15

Table 4: Mechanical properties of EN AW-6082 T6 (EN755-2, 2016)

Wall thickness, t (mm)	Yield stress $R_{p0,2}$ (MPa)	Tensile strength R_m (MPa)	Elongation		Hardness HB
			A (%)	A _{50mm} (%)	
≤ 5	250	290	8	6	95
5 < t ≤ 25	260	310	10	8	95

Experimental testing of CHS profiles made from alloy EN AW-6082 T6 was done by Đuričić et al. In this experiment 0,2 % proof strength (f_0), ultimate tensile strength (f_u) and elongation for the material was investigated as well as two intermediate stresses ($f_{1\%}, f_{3\%}$). This gave engineering stress values for Ø50x2 mm and Ø20x2 mm shown in Table 5 (Đuričić et al., 2017).

Table 5: Engineering stress-strain relations (Đuričić et al., 2017)

Profile(mm)	f_0 (MPa)	$f_{1\%}$ (MPa)	$f_{3\%}$ (MPa)	f_u (MPa)	Elongation (%)
Ø50x2	309,34	333,69	339,42	342,48	5,56
Ø20x2	272,34	283,51	289,09	304,38	5,67

Elastic modulus for EN AW-6082 T6 is 69500 MPa (Đuričić et al., 2017).

2.1.4 Heat-affected zone

When welding aluminium alloy members, the generated heat will reduce the material properties near the welds. The yield strength in the heat affected zones is approximately one half of the original material yield strength and it is important to know the extent of heat-affected softening for design of a structure (Müller, 2011).

According to Eurocode 9 part 1-1, the heat-affected zone should be considered for the 6xxx-series in temper T4 and above. Eurocode 9 gives the characteristic values of 0,2 % proof strength ($f_{0,HAZ}$) and ultimate tensile strength ($f_{u,HAZ}$) for heat-affected zones in alloy EN AW-6082 T6 (EN1999-1-1, 2007).

$$f_{0,HAZ} = 125 \text{ N/mm}^2$$

$$f_{u,HAZ} = 185 \text{ N/mm}^2$$

A method to experimentally achieve values for the heat-affected zone is proposed by Metusiak, as described by Wang. This consists of measuring Vickers hardness of heat-affected zone and using the relation showed in the following formulas, between Vickers hardness and yield and ultimate stresses (Matusiak, 1999, Wang, 2006).

$$f_{0,2}(\text{MPa}) = 3,6HV - 81 \tag{1}$$

$$f_u(\text{MPa}) = 2,6HV + 54 \tag{2}$$

Where:

HV is the Vickers hardness

$f_{0,2}$ (MPa) is the 0,2 % proof strength (MPa)

f_u (MPa) is the ultimate tensile strength (MPa)

A different approach to achieve values from Vickers hardness was proposed by Myhr and Grong, as described by Đuričić. This approach gives lower values than the approach mentioned above (Đuričić et al., 2017).

$$f_{0,2}(MPa) = 3HV - 48,1 \quad (3)$$

$$f_u(MPa) = 2,6HV + 39,8 \quad (4)$$

Đuričić et al. measured Vickers hardness in two different heat-affected zones. Vickers hardness is measured according to description in EN ISO 6507-1 (2005). Material within 20 mm of the weld is assigned HAZ1 and HAZ2 consist of material within 10 mm of HAZ1. Expression (3) and (4) are used to calculate 0,2 % proof stresses and ultimate strengths. The above results are presented in Table 6 (Đuričić et al., 2017).

Table 6: Stresses of material in HAZs (Heat affected zones) (Đuričić et al., 2017)

Zone	HV	$f_{0,haz}$ (MPa)	$f_{u,haz}$ (MPa)
HAZ 1	62	137,90	201,00
HAZ 2	75	176,90	234,80

2.2 Stress-strain relationship

Eurocode 9 part 1-1 (Annex E) describes the stress-strain relationship with piecewise linear models. Piecewise linear models are based on Hooke's law for each of the lines representing the stress-strain relationship. Each line is represented with a different hardening modulus. These models will increase in accuracy as the number of lines is increased. This can be illustrated with a bi-linear model and a three-linear model. For the bi-linear model the following relationship can be assumed (EN1999-1-1, 2007).

$$\sigma = E\varepsilon \quad \text{for } 0 < \varepsilon \leq \varepsilon_p \quad (5)$$

$$\sigma = f_p + E_1(\varepsilon - \varepsilon_p) \quad \text{for } \varepsilon_p < \varepsilon \leq \varepsilon_{max} \quad (6)$$

$$E_1 = \frac{f_{max} - f_p}{\varepsilon_{max} - \varepsilon_p} \quad (7)$$

Where:

f_p is the elastic limit of proportionality (Pa)

ε_p is the strain corresponding to the stress f_p

f_{max} is the maximum stress of the material (Pa)

ε_{max} is the strain corresponding to the stress f_{max}

E is the elastic modulus (Pa)

E_1 is the first hardening modulus (Pa)

For the three-linear model an additional stress-strain is added in the diagram and following relationships can be assumed (EN1999-1-1, 2007).

$$\sigma = E\varepsilon \quad \text{for } 0 < \varepsilon \leq \varepsilon_p \quad (8)$$

$$\sigma = f_p + E_1(\varepsilon - \varepsilon_p) \quad \text{for } \varepsilon_p < \varepsilon \leq \varepsilon_e \quad (9)$$

$$\sigma = f_e + E_2(\varepsilon - \varepsilon_e) \quad \text{for } \varepsilon_e < \varepsilon \leq \varepsilon_{max} \quad (10)$$

$$E_1 = \frac{f_e - f_p}{\varepsilon_e - \varepsilon_p} \quad (11)$$

$$E_2 = \frac{f_{max} - f_e}{\varepsilon_{max} - \varepsilon_e} \quad (12)$$

Where:

f_e is the limit of elasticity (Pa)

ε_e is the strain corresponding to the stress f_e

E_2 is the second hardening modulus (Pa)

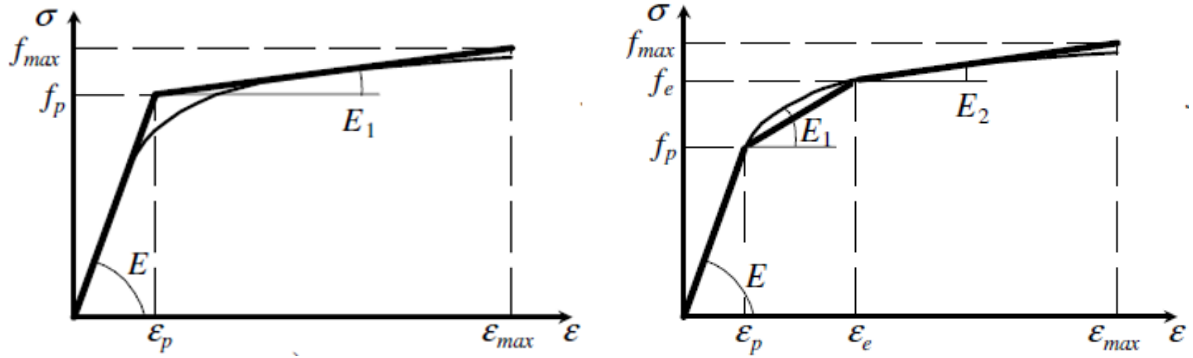


Figure 1: Bi-linear model (left) and three-linear model (right) of stress-strain relationship (EN1999-1-1, 2007)

From the 0,2 % proof strength, which is the conventional value for f_0 , the elastic limit of proportionality (f_p) can be calculated with the formula (EN1999-1-1, 2007):

$$f_p = f_0 - 2\sqrt{10f_0} \quad \text{if } f_0 > 160 \text{ N/mm}^2 \quad (13)$$

$$f_p = f_0/2 \quad \text{if } f_0 \leq 160 \text{ N/mm}^2 \quad (14)$$

Where:

f_0 is the 0,2 % proof strength (Pa)

Calculating the axial stress (σ) of a specimen is done by dividing the axial load (P) by the cross-sectional area (A). If the initial area (A_0) is used, the engineering stress is obtained. When a specimen is in tension the actual area of the cross-section is less than the initial area. By dividing the axial load on the tensioned area, a larger stress will be obtained. This is called true stress (Gere, 2004).

Engineering stress-strains can be converted into true stress-strains with the following approximations (Đuričić et al., 2017):

$$\varepsilon = \ln(1 + \varepsilon_{eng}) \quad (15)$$

$$\sigma = \sigma_{eng}(1 + \varepsilon_{eng}) \quad (16)$$

Where:

ε_{eng} is the engineering strain

σ_{eng} is the engineering stress (Pa)

2.3 Design of K-joints

2.3.1 Failure modes

According to Eurocode 3, part 1-8, the failure modes that should be considered for hollow section joints, illustrated in Figure 2, are (EN1993-1-8, 2005):

- a) Chord face failure, or chord plastification:
Plastic failure of chord face or of the chord cross-section
- b) Chord side wall failure:
Yielding, crushing or instability under the compression brace member, by crippling or buckling of the chord side wall.
- c) Chord shear failure:
Shear failure in the chord
- d) Punching shear failure:
By crack initiation leading to rupture of the brace members from the chord member
- e) Brace failure:
Reduced effective width causing cracking in the welds or in the brace members
- f) Local buckling:
Buckling failure of a brace member or chord member at the joint location


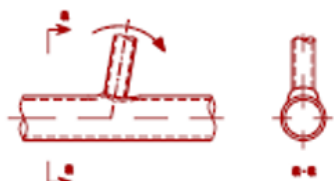
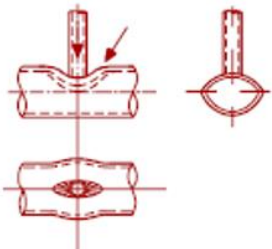
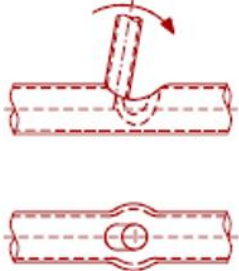
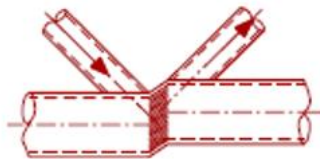
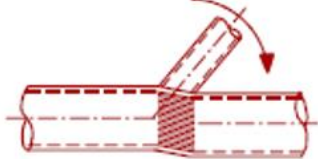



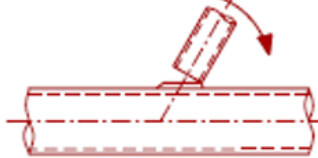
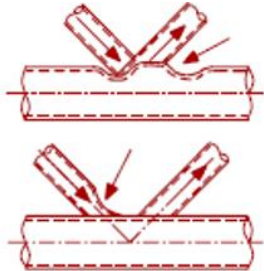

Mode	Axial loading	Bending moment
a		
b		
c		
d		
e		
f		

Figure 2: Failure modes for joints made of CHS-profiles (EN1993-1-8, 2005)

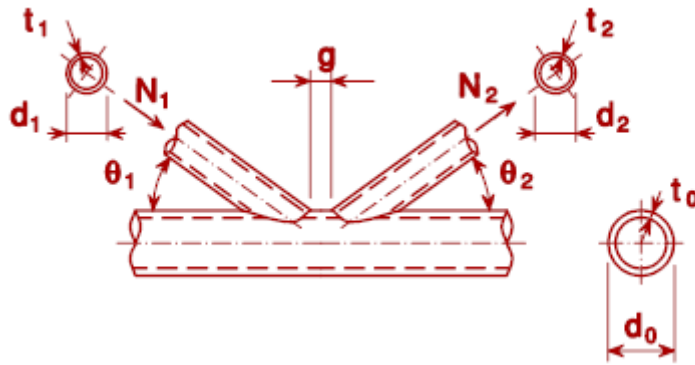


Figure 3: Gap K-joint with geometric sizes (EN1993-1-8, 2005)

Geometric sizes of a gap K-joint is given in Figure 3. If these sizes are in the range of validity given in Table 7, only chord face failure and punching shear needs to be considered (EN1993-1-8, 2005).

Table 7: Validity range for welded joints between CHS brace members and CHS chords (EN1993-1-8, 2005)

$0,2 \leq \frac{d_i}{d_0} \leq 1,0$
$10 \leq \frac{d_0}{t_0} \leq 50$
$\frac{d_i}{t_i} \leq 50$
$g \geq t_1 + t_2$

Additional to validity range in Table 7 the angle of the brace members should be higher than 30° to ensure proper welds between chord and braces (Wardenier, 2001).

2.3.2 Design axial resistances for K-joints

Eurocode 3 part 1-8 suggests models for the calculations of axial resistances of brace members ($N_{1,Rd}$, $N_{2,Rd}$) against chord face failure and punching shear failure in a K-joint (EN1993-1-8, 2005).

- **Chord face failure**

$$N_{1,Rd} = \frac{k_g k_p f_{y0} t_0^2}{\sin \theta_1} \left(1,8 + 10,2 \frac{d_1}{d_0} \right) / \gamma_{M5} \quad (17)$$

$$N_{2,Rd} = \frac{\sin \theta_1}{\sin \theta_2} N_{1,Rd} \quad (18)$$

Where:

$$k_g = \gamma^{0,2} \left(1 + \frac{0,024 \gamma^{1,2}}{1 + \exp\left(\frac{0,5g}{t_0} - 1,33\right)} \right) \quad (19)$$

$N_{1,Rd}$ is the resistance force in compressed brace member (N)

$N_{2,Rd}$ is the resistance force in tensioned brace member (N)

f_{y0} is the yield strength of chord (Pa)

t_0 is the thickness of chord (m)

θ_1 is the angle between compressed brace member and chord member (°)

θ_2 is the angle between tensioned brace member and chord member (°)

d_1 is the diameter of compressed brace member (m)

d_0 is the diameter of chord member (m)

γ_{M5} is the partial safety factor for resistance of joints in hollow section lattice girder, $\gamma_{M5} = 1,0$ (EN1999-1-1, 2007)

k_g is the joint geometry factor

γ is the ratio of brace member to twice its wall thickness

g is the gap between brace members (m)

k_p is the chord stress factor, $k_p = 1,0$ for k-joints without pre-loading (EN1993-1-8, 2005)

- **Punching shear failure**

$$N_{i,Rd} = \frac{f_{y0}}{\sqrt{3}} t_0 \pi d_i \frac{1 + \sin \theta_i}{2 \sin^2 \theta_i} / \gamma_{M5} \quad (20)$$

Where:

d_i is the diameter of brace member i (m)

2.3.3 Aluminium softening reduction factor

In case of material characteristics not being affected by welding heat, resistance is higher than in the case of softening in heat affected zones. In case of completely softened joint there is a lower resistance than the experimental case. The aluminium softening for the design resistance is taken into account by introducing the aluminium softening reduction factor, k_{al} (Đuričić et al., 2017).

$$N_{1,Rd,Al} = k_{al} \frac{k_g k_p f_{y0} t_0^2}{\sin \theta_1} \left(1,8 + 10,2 \frac{d_1}{d_0} \right) / \gamma_{M5} \quad (21)$$

To determine k_{al} the softening zone is defined with strength reduction factor, $\rho_{0,haz}$, determined by the expression:

$$\rho_{0,haz} = \frac{f_{0,haz}}{f_0} \quad (22)$$

Where:

$f_{0,haz}$ is the yield strength for material in HAZ (Pa)

f_0 is the yield strength for material not in HAZ (Pa)

The size of the softening zone is called b_{HAZ} . This varies for different types of thicknesses and welding techniques. For a TIG weld on a material with thickness between 0 and 6 mm, b_{HAZ} has a value of 30 mm. This length is set to be from the weld and 30 mm along the material (EN1999-1-1, 2007).

For a K-joint made from circular tubes, the cross section having the largest HAZ surface is considered. The total length of the softening zone L^* is the circular arc of the chord that is in the softening zone. This consist of two parts, the arc length inside the brace member (l) and one part outside of the brace member with length $2b_{HAZ}$. The total circumference of the chord is called L . The expression for k_{al} in a K-joint made from CHS profiles is (Đuričić et al., 2017):

$$k_{al} = 1 - \frac{(1-\rho_{0,haz})L^*}{L} \quad (23)$$

Where:

$\rho_{0,haz}$ is the strength reduction factor for heat affected zone

L^* is the total softening zone arc length in the cross-section having the largest HAZ surface (m)

L is the circumference of the chord member cross-section (m)

2.4 Previous analysis of k-joints

Deformation limit proposed by Lu et al. (1994)

According to Lu et al. as described by Choo et al. there are two limit strengths in a CHS joint, the ultimate strength, N_u , and the serviceability strength, N_s . A chord indentation of $\Delta_u = 0,03d_0$ corresponds to N_u , while N_s corresponds to chord indentation of $\Delta_s = 0,01d_0$. If there is a peak in the load-deformation diagram, this deformation will be used as the ultimate deformation limit if it is lower than $0,03d_0$. This study suggests that for CHS joints the ultimate deformation limit is the one governing the strength of the structure (Lu et al., 1994, Choo et al., 2003).

Research study of aluminium trusses by van Hove and Soetens (2016)

Van Hove and Soetens studied welded joints in a 30-meter span aluminium truss. Their truss consisted of K- and N-joints. This study investigated the possibility to apply design rules for steel, since there are no rules for aluminium design. The study consisted of a numerical analysis of the welded connections as well as a testing experiment to verify the numerical model. The material used in this analysis was aluminium alloy 6082 T6. They concluded that for both chord and brace sizes, the N-joints were governing. Further, the study concluded that failure mode and behaviour of aluminium joints are well predicted by the steel design rules. However, the failure load is overestimated by 8% for the truss that was investigated (van Hove and Soetens, 2016).

Experimental study of aluminium k-joints by Đuričić et al. (2017)

Đuričić et al. investigated three different k-joints made of aluminium alloy 6082 T6. This study consisted of a numerical analysis, experimental testing and hand calculations. Two different approaches for calculation of joint resistance was discussed in this study. One of them is to use the steel design rules found in EN1993-1-8, explained in chapter 2.3. The other approach is received from a previous study from Wardenier. The general expression for chord plastification for this approach is (Đuričić et al., 2017, Wardenier, 2001):

$$N_1 = f(\beta)f(\gamma)f(g')\frac{f_{y0}\cdot t_0^2}{\sin(\theta_1)}f(n') \quad (25)$$

Where:

$f(\beta)$, $f(\gamma)$ and $f(g')$ are functions dependent on the joint members geometry

$f(n')$ is a function of the chord pre-load

f_{y0} is the chord yield stress (Pa)

t_0 is the thickness of the chord (m)

θ_1 is the angle between chord and compressed brace member (°)

Conclusion in this study is that with the use of aluminium softening reduction factor, k_{al} , explained in chapter 2.3.3, the analytical solution and the numerical and experimental analysis have a satisfactory match (Đuričić et al., 2017).

2.5 The finite element method

The principal of the finite element method is to divide a complex problem into several simpler problems and with the help of mathematics connect all the simple problems into an approximate solution of the original complex problem (Mac Donald, 2007). The logical diagram in Figure 4 presents the process of finite element analysis.

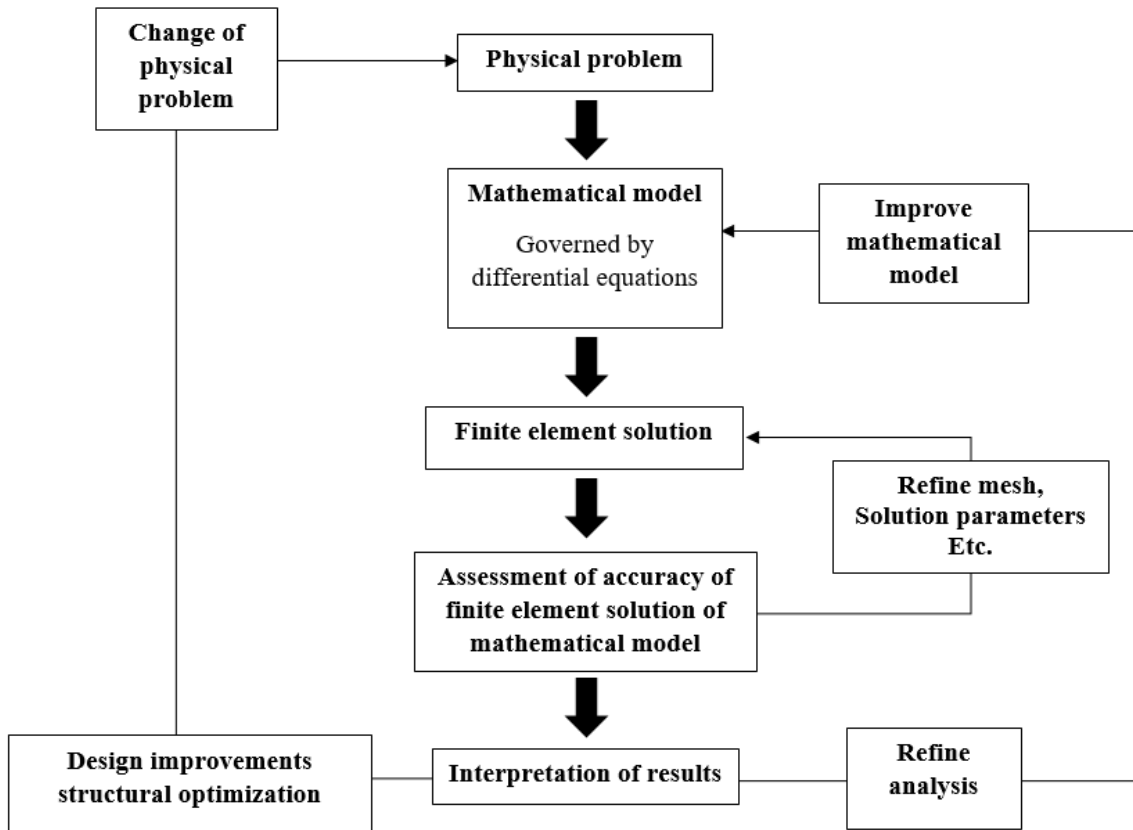


Figure 4: Logical diagram of the process of finite element analysis(Bathe, 2006)

Finite element analysis is introduced to examine physical problems that are too complex to examine just by using simple theoretical solutions. These problems include complex structures with many different cross-sections and loads, and structures with complicated geometry. To idealize the physical problem to a mathematical model some assumptions are required. These are made on the geometry, kinematics, materials, loading and boundary conditions. Then the mathematical model is formed, which is governed by differential equations. It is this mathematical model the finite element method solves. To solve this model, it is necessary to divide it into several smaller elements called finite elements. The size of the elements, known as mesh size, controls the accuracy of the solution. If the solution is not sufficiently accurate then it is necessary to repeat the numerical analysis with refined solution parameters, such as mesh size, until accuracy criteria are met. If the finite element solution is accurate then it converges to the exact solution as the number of elements is increased. Results from the analysis are interpreted and in case of insufficient accuracy, the aforementioned procedure is repeated (Bathe, 2006).

2.5.1 Boundary conditions and loading

It is important to consider which boundary and loading conditions must be used when building a model. The loads and constraints can be applied directly to the nodes. However, in solid modelling this can cause large stresses and local failure near the loaded or constrained nodes. For solid modelling it is recommended to apply the loads and constraints to areas. This reduces the chance of local failure and the mathematical model is more realistic in relation to the real physical problem (Bathe, 2006).

2.5.2 Linear analysis

A linear analysis is performed when the material considered as linearly elastic, the displacements are infinitesimally small and the nature of the boundary conditions remain unchanged during the application of the loads on a finite element model. The equilibrium equations for a static analysis are:

$$\mathbf{KU} = \mathbf{R} \quad (26)$$

Where:

K is the stiffness matrix (N/m)

U is the displacement vector (m)

R is the load vector (N)

These equations show a linear relation between load vector **R** and the displacement response **U** (Bathe, 2006).

2.5.3 Nonlinear analysis

When the assumptions in 2.5.2 are not used, a nonlinear analysis must be performed.

Nonlinear analyses can be categorized into different types based on which assumptions are used. These types are (Bathe, 2006):

- Materially nonlinearity only:
 Infinitesimal displacements and strains with a nonlinear stress-strain relation
- Large displacements, large rotations, but small strains:

Displacement and rotations of fibres are large, but extensions and angle changes between fibres are small, both linear and nonlinear stress-strain relations can be used.

- Large displacements, large rotations, and large strains:

Extensions and angle changes between fibres are large, both linear and nonlinear stress-strain relations can be used.

When performing a nonlinear analysis, it is important to consider which of the categories the physical problem is classified as. Even though the most general large strain formulation will give accurate results, it may be more efficient computationally to select a more restrictive formulation (Bathe, 2006).

2.6 ANSYS Mechanical APDL

ANSYS is a modelling package for solving mechanical problems with finite element method. The mechanical problems include: static and dynamic structural analysis, heat transfer, fluid problems, acoustic problems and electro-magnetic problems. The static and dynamic structural analysis include both linear and non-linear analysis (ANSYS, version 18.2, Academic).

2.6.1 Element type used in ANSYS

For solid modelling in ANSYS with complicated geometry element type SOLID285 can be used. SOLID285 is a tetrahedral 4-node structural solid element. The element is defined by four nodes with four degrees of freedom each, translation in x, y and z direction and one hydrostatic pressure. The geometry of the SOLID285 element with node location and coordinate system is displayed in Figure 5. The element has plasticity, hyperelasticity, creep, stress stiffening, large deflection and large strain capabilities. Input data for the element includes isotropic, orthotropic and anisotropic material properties (ANSYS, version 18.2, Academic).

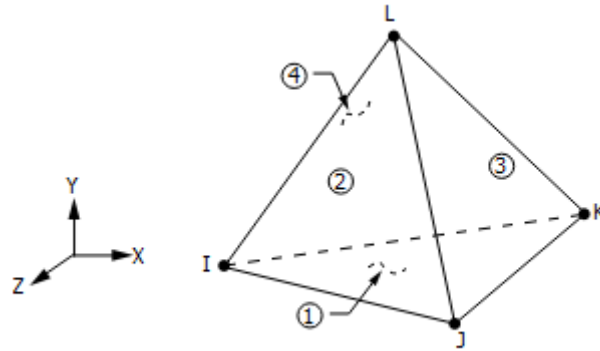


Figure 5: Geometry of SOLID285 element (ANSYS, version 18.2, Academic)

2.6.2 Element size and Meshing

When making elements in ANSYS the size of the elements must be taken into consideration. To set element sizes there are different functions that can be used. The size of the element edge size can be set directly with the ESIZE function. A different function is to use SMRTSIZE. With this function the software will create element sizes based on the geometry of the structure and the input size level. The size level is a number between 1 and 10 with 1 as the finest mesh and 10 as the coarsest mesh. There are also options of mapped or free meshing. Mapped meshing gives uniform elements through the whole structure but can be difficult to use in complicated geometries. Free meshing is not restricted to certain shapes and can be better to use for complex geometries. Meshing a structure is done by meshing functions LMESH, AMESH or VMESH based on which elements are present (ANSYS, version 18.2, Academic).

2.6.3 Multilinear isotropic hardening (TB,MISO)

Multilinear isotropic hardening is a model used for describing stress-strain relationships in ANSYS. The function TB,MISO creates a table with input of strain (ϵ), and stress (σ) corresponding to this strain using TBPT command. Materials assigned to these tables will follow the deformation curves of the assigned values (ANSYS, version 18.2, Academic).

3 Methodology

3.1 Introduction

The first part of the modelling process was dedicated to learning the software. This included reading and practicing on tutorials, starting with simple models and advancing to more complicated models. Parallel to this, different databases were researched and the experimental data in Đuričić et al. (2017) were selected for the verification of the numerical analysis. This was used as a base for all numerical modelling in this thesis. It was also investigated how to calculate design resistance in the different models and the approach from Eurocode 3, part 1-8 (2005) was selected. When all preparations were finished, the model that would be compared to experimental data was developed using computer software ANSYS 18.2. After this, models containing different parameters were constructed using the same input as the reference model, only changing one parameter at the time. Since a K-joint often has the same angle between both brace members and chord, it was decided to change both angles for the models. For modelling purposes, the weld was simplified. The braces were modelled as fixed to the chord member, without the fillet weld being modelled.

3.2 Different K-joints to be modelled

Table 8: Different models to investigate

Model number	Chord profile	Brace profile	Angle ($\theta_1 = \theta_2$)
1	Ø50x2 mm	Ø20x2 mm	45°
2	Ø50x2 mm	Ø20x2 mm	30°
3	Ø50x2 mm	Ø20x2 mm	60°
4	Ø20x3 mm	Ø20x2 mm	45°

The experimental data from Đuričić et al. (2017) were used for model number 1. The members' lengths were selected in order to avoid buckling of compressed brace member. In all models compressed brace member had length equal to 150 mm, tensioned brace member had length equal to 300 mm and chord had length equal to 750 mm. Since they were welded connections in aluminium under examination there was a need to consider the effect of the heat affected

zone. Data for two heat affected zones were obtained from the experimental analysis and implemented in the models. Geometry of the model is depicted in Figure 6.

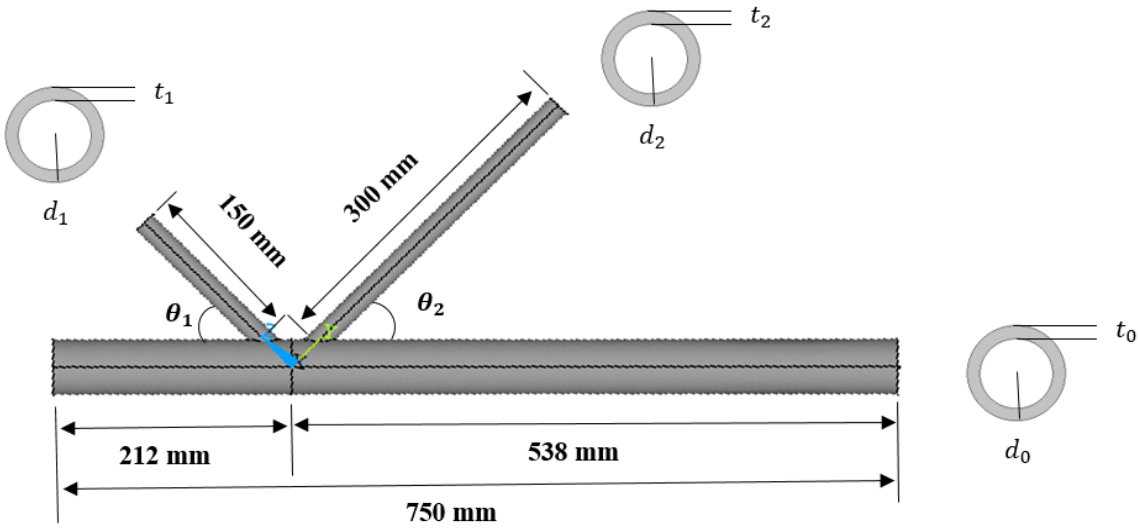


Figure 6: Geometry of investigated models

3.3 Numerical analysis

3.3.1 Geometry

The geometry presented in chapter 3.2 was modelled in ANSYS with the help of simple solid cylinder functions. Split functions were used to make the curved shape of the braces at the intersection with the chord. The braces and chord were added together as a single volume to make them fixed, in order to simulate the weld. Symmetry conditions were applied to the structure, since stresses and deformations would be the same at both sides of the symmetry axis. Initial geometry of the structure with brace angle of 45°, as constructed in ANSYS, can be viewed in Figure 7.

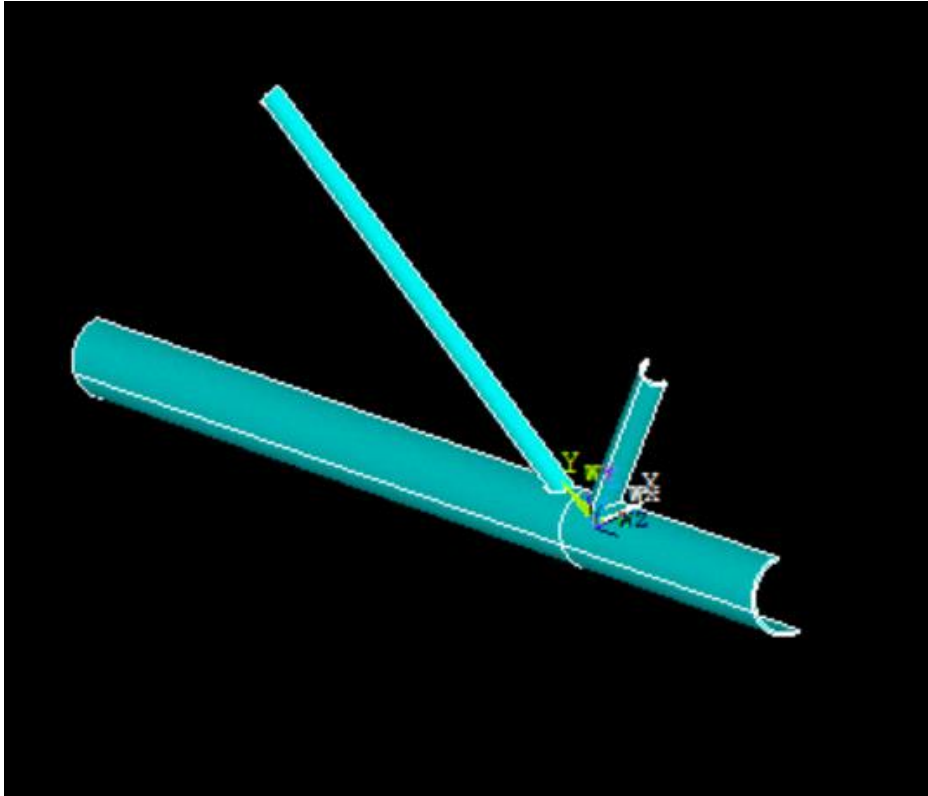


Figure 7: Initial model of k-joint with angle of 45 degrees

3.3.2 Element selection and meshing

The structures have a solid geometry and the selection of finite elements is important. A large variety of elements in ANSYS were investigated and SOLID285 element type was selected. SOLID285 has a tetrahedral shape which makes it optimal for structures with irregular shapes. Elements with more nodes than SOLID285 can be found in ANSYS library. They offer some advantages over SOLID285 but since an academic version with node limitations is used, it was decided to apply SOLID285. To make models that will give a realistic solution it was decided to make a finer mesh in the vicinity of the connection and coarser mesh in the parts with a further distance to the connection. This was done by creating a different volume around the weld. All volumes within 100 mm of the centre of the connection were defined as a new volume.

Due to the complexity of the geometry of the K-joint, it was decided to use free meshing for the model. To select mesh sizes, the function SMRTSIZE was used. The volume furthest from the connection center was assigned a size level 10, and the volume closest to the connection was assigned size level 2. Each volume was meshed by itself using VMESH with the different size levels assigned. The resulting mesh responded well during the analysis. The meshed model is shown in Figure 8.

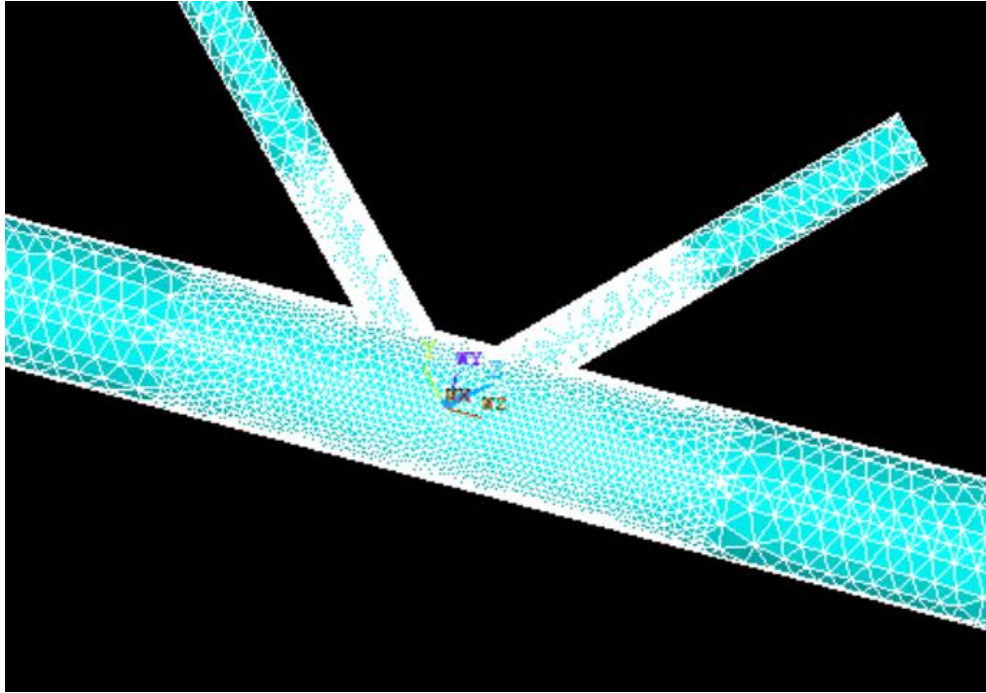


Figure 8: Mesh of k-joint

3.3.3 Material input

For all parts of the structure, the aluminium alloy EN AW-6082 T6 was used. Material properties was obtained from the experimental data in Đuričić et al. (2017). Value of elastic modulus was set as 69500 MPa and Poisson's ratio was set as 0,33 for all materials.

- Chord and brace members

Đuričić et al. (2017) completed tests to investigate stress-strain relationship in the different CHS profiles. Among these tests, the chord profile and brace profile used in this thesis were investigated. The test showed engineering stresses for 0,2 % proof stress, 1 % tensile stress, 3 % tensile stress and ultimate tensile strength as well as ultimate elongation. Equation (15) and (16) are applied to calculate the true stresses shown in Table 9.

Table 9: True stresses in CHS profile

Profile(mm)	f_0 (MPa)	$f_{1\%}$ (MPa)	$f_{3\%}$ (MPa)	f_u (MPa)	Elongation (%)
Ø50x2	311,3	337,0	349,6	361,9	5,51
Ø20x2	274,0	286,3	297,8	321,6	5,52

- **Heat affected zones**

Đuričić et al. (2017) measured Vickers hardness in two zones of the heat-affected zone. One zone from weld and 20 mm along the material, and the second one from the edge of zone 1 and 10 mm along the material. The difference in hardness created two different engineering stress-strain relationships in the two zones. True stresses and strains are calculated from equation (15) and (16) Values for engineering and true stresses are showed in Table 10.

Table 10: Stresses for heat affected zones

Zone	HV	Engineering stress		True stress	
		$f_{0,eng}$ (MPa)	$f_{u,eng}$ (MPa)	$f_{0,true}$ (MPa)	$f_{u,true}$ (MPa)
HAZ1	62	137,9	201,0	138,4	211,9
HAZ2	75	176,9	234,8	177,7	247,5

All the models were assigned HAZ1 and HAZ2. This was done by creating three points on the weld, one at the right side of the brace, one at the left side of the brace and one at the middle. All the elements within a distance of 20 mm from the points were assigned to HAZ1, and all the elements within a distance between 20 mm and 30 mm from the points were assigned to HAZ2.

3.3.4 Stress-strain curves

Values from 3.3.3 were assigned to different materials with multilinear isotropic hardening tables, which created deformation path curves. For chord and braces the points consisted of 0,2 % proof strength, 3 % tensile strength, ultimate tensile strength and the elastic limit of proportionality calculated from expression (13) and (14). For the heat affected zones 0,2 % proof strength, ultimate strength and elastic limit of proportionality were used.

Table 11: Multilinear isotropic hardening table for $\varnothing 50 \times 2$ mm in ANSYS

Point number	Strain (ϵ)	Stress (σ) (MPa)
1	0,00287	199,74
2	0,00643	311,34
3	0,0296	349,60
4	0,0551	361,86

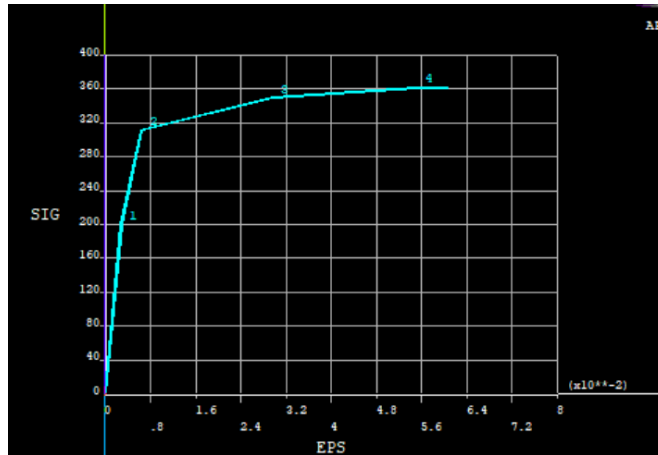


Figure 9: Plot of Ø50x2 mm stress-strain curve

Table 11 and Figure 9 presents the input multi linear isotropic table in ANSYS and the stress-strain diagram for CHS-profile Ø50x2 mm.

Table 12: Multilinear isotropic hardening table for Ø20x2 mm in ANSYS

Point number	Strain (ϵ)	Stress (σ) (MPa)
1	0,00242	169,27
2	0,00592	273,95
3	0,0296	297,76
4	0,0552	321,64

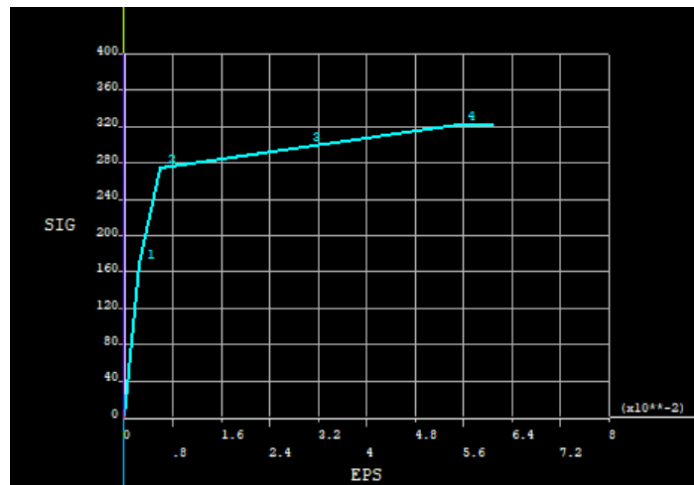


Figure 10: Plot of Ø20x2 mm stress-strain curve

Table 12 and Figure 10 presents the input multi linear isotropic table in ANSYS and the stress-strain diagram for CHS-profile Ø20x2 mm.

Table 13: Multilinear isotropic hardening table for HAZ1 in ANSYS

Point number	Strain (ϵ)	Stress (σ) (MPa)
1	0,000992	69,22
2	0,00398	138,45
3	0,0527	211,88

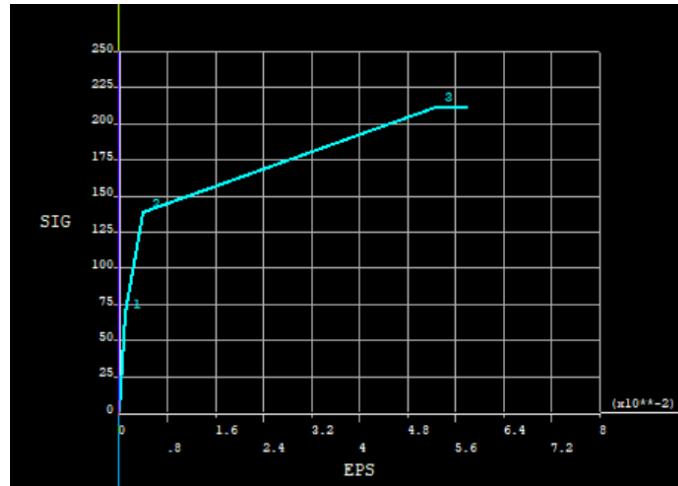


Figure 11: Plot of HAZ1 stress-strain curve

Table 13 and Figure 11 presents the input multi linear isotropic table in ANSYS and the stress-strain diagram for HAZ1.

Table 14: Multilinear isotropic hardening table for HAZ2 in ANSYS

Point number	Strain (ϵ)	Stress (σ) (MPa)
1	0,00134	93,39
2	0,00454	177,70
3	0,0527	247,50

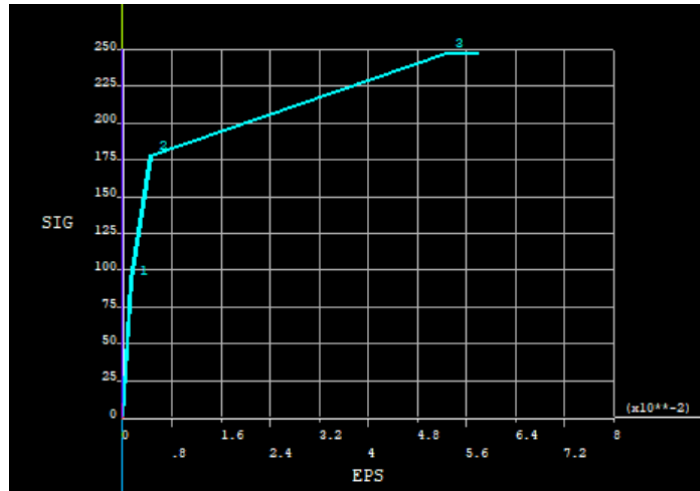


Figure 12: Plot of HAZ2 stress-strain curve

Table 14 and Figure 12 presents the input multi linear isotropic table in ANSYS and the stress-strain diagram for HAZ2

3.3.5 Boundary conditions and loads

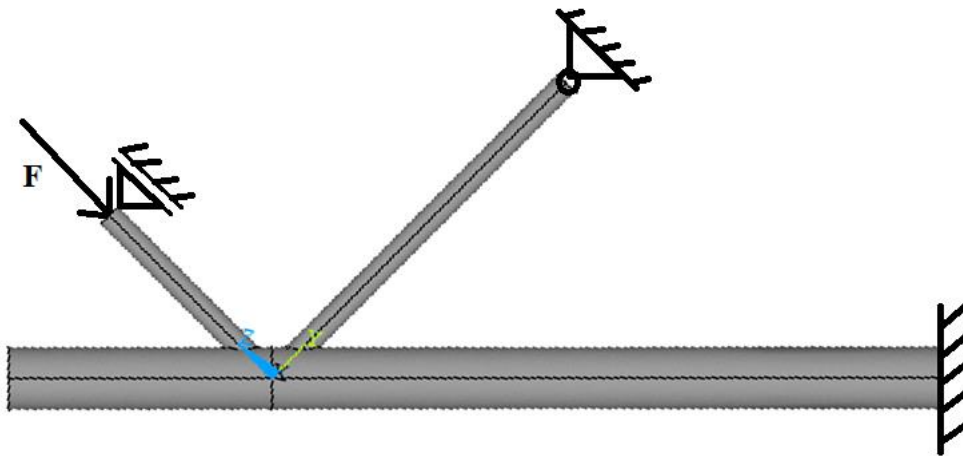


Figure 13: Structure with applied boundary conditions and loading

The model was constrained in the same way as the experimental testing as shown in Figure 13. One end of the chord was free while the end furthest from the connection was fixed and could not be displaced in any direction or rotation. The end of the tensioned brace was pinned so that it could not move in any direction, but it was free to rotate. The end of the compressed brace member was constrained so it could only move in the direction of the applied force. All areas at the symmetry axis were constrained with symmetry constraints. Constraints were applied on areas to avoid local failure around constrained parts of the model. Load was applied as pressure

at the top of the compressed brace and had different values for the models. Table 15 presents the pressure applied and the corresponding force.

Table 15: Pressure applied on compressed brace

Model	Pressure (MPa)	Force (kN)
1	147,47	16
2	176,83	20
3	132,63	15
4	212,20	24

3.3.6 Analysis type and postprocessing

Last step of modelling was to select analysis type static, turn on the large deformation analysis and set time steps. The time step was set to 0,05 which resulted in 20 iterations. The use of more iterations has been examined but the results obtained changed insignificantly so 20 iterations were chosen as a sufficient number. When the whole model was complete the solution process could be initiated. The solution time was about 5 minutes for each model.

The largest deformation was found where the compressed brace is in contact with chord face. At this point there was measured deformation normal to the chord face. Deformation in the same direction was measured at two points 50 mm away from the point of maximal deformation. Average deformation of these two points was considered to be total shift at the point of maximal deformation and was subtracted from the maximal deformation, in that way only chord indentation was measured.

3.4 Interpretation of numerical results

After detailing and repeating numerical process, model 1 gave results that were comparable to the experimental data obtained from Đuričić et al. (2017). Force-deformation curves were developed from all models and ultimate strength and serviceability strength were obtained for the models with chord member thickness of 2 mm, according to chapter 2.4. For the model with chord thickness 3 mm, deformation above the limits set by Lu et al. (1994) was not obtained so the peak of the graph is selected as ultimate strength. Obtained strengths from the different

models was compared to each other to investigate how the change of angle and chord influenced the strength.

3.5 Hand calculations of K-joint

The calculation approach as described in chapter 2.3 was used. Hand calculations were done in two parts. First, where heat-affected zone was not taken into consideration, and secondly, where heat-affected zone was a part of the calculation.

3.5.1 Calculations without consideration of heat affected zone

In these calculations only yield strength of the chord material was used. Equation (17) was used to calculate design resistance in compressed brace member, $N_{1,Rd}$, against chord face plastification. Design resistance of tensioned brace member was the same, since $\theta_1 = \theta_2$. Punching shear resistance was also calculated with equation (20). Yield stress obtained from Đuričić et al. (2017) and from Eurocode 9 was used to calculate design resistance. Equation (19) was used to calculate k_g . $k_p = 1$ for joints without chord pre-stress and $\gamma_{M5} = 1$ is partial safety factor for resistance of joints in hollow section lattice girder. The calculations are shown in Table 16. Resistance for chord plastification has the index cp, resistance for punching shear is indexed ps and resistances with yield strength obtained from Eurocode 9 is indexed EN.

Table 16: Calculations according to Eurocode 3 part 1-8

Model	1	2	3	4
k_g	1,657	1,657	1,668	1,529
k_p	1	1	1	1
f_{y0} (MPa)	311,34	311,24	311,34	311,34
$f_{y0,EN}$ (MPa)	250	250	250	250
t_0 (mm)	2	2	2	3
θ_1 (°)	45	30	60	45
d_1 (mm)	20	20	20	20
d_0 (mm)	50	50	50	50
γ_{M5}	1	1	1	1
$N_{1,Rd,cp}$ (kN)	17,2	24,2	14,0	35,5
$N_{1,Rd,cp,EN}$ (kN)	13,8	19,5	11,3	28,6
$N_{1,Rd,ps}$ (kN)	38,5	67,8	28,1	57,8
$N_{1,Rd,ps,EN}$ (kN)	31,0	54,4	22,6	46,4

3.5.2 Calculations with consideration of heat affected zone

Chapter 3.5.1 shows that the design resistance is the resistance related to chord plastification. Further calculations are therefore only chord plastification resistance. In case of completely softened joint, EN1999-1-1 (2007) states yield resistance, $f_{y0,haz} = 0,5 * f_{y0}$. Since cross section is not completely softened this will give too low values for joint resistance. To calculate resistance of partially softened joint, equation (21) is used. For this aluminium softening coefficient, k_{al} , must be defined with equation (23). Calculations on k_{al} are based on the cross-section of the chord with the largest amount of heat affected material. At this cross-section the arc length of the heat affected zone, L^* , is the extent of zone, b_{HAZ} , on both sides of the brace and the arc length within the brace member, l , illustrated in Figure 14.

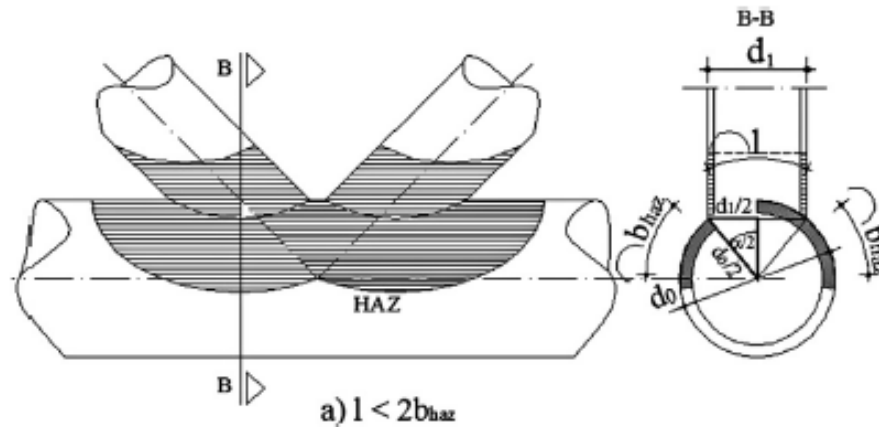


Figure 14: Extent of heat affected zone (Đuričić et al., 2017)

Eurocode 9 gives b_{HAZ} to be 30 mm for TIG welding. Length within the brace member, l , is given by the angle $\alpha = 2\arcsin(\frac{d_1/2}{d_0/2})$, where $l = \frac{\alpha}{360} * \pi d_0$. Total circumference of chord is $L = \pi d_0$. To calculate $\rho_{0,haz}$, equation (22) is applied. In the experimental data there are two different yield stresses in the heat affected zone while Eurocode 9 only describe one. For these calculations the average value of yield stress, $f_{y0,HAZ,av}$, through the whole heat affected zone is used. Calculation of design resistances for fully softened cross-section ($N_{1,Rd,HAZ}, N_{1,Rd,HAZ,EN}$) and for partially softened cross-section ($N_{1,Rd,Al}, N_{1,Rd,Al,EN}$) are shown in Table 17.

Table 17: Calculation of design resistance of softened cross-section

Model	1	2	3	4
α (°)	47,16			
l (mm)	20,58			
b_{HAZ} (mm)	30			
L^* (mm)	80,58			
L (mm)	157,08			
$f_{y0,HAZ,av}$ (MPa)	147,65			
$f_{y0,HAZ,EN}$ (MPa)	125			
$\rho_{0,Haz}$	0,477			
$\rho_{0,Haz,EN}$	0,5			
k_{al}	0,732			
$k_{al,EN}$	0,744			
$N_{1,Rd,HAZ}$ (kN)	8,58	12,08	7,02	17,73
$N_{1,Rd,HAZ,EN}$ (kN)	6,89	9,74	5,66	14,30
$N_{1,Rd,Al}$ (kN)	12,56	17,68	10,28	25,96
$N_{1,Rd,Al,EN}$ (kN)	10,25	14,49	8,42	21,27

3.5.3 Comparison of numerical results and hand calculations

The results from hand calculations were compared to the numerical results. Calculation results were divided by ultimate strength limit from numerical results to investigate if they correspond to each other. It was also interesting to investigate if the hand calculations gave the same relation to design resistance when changing the angle of the chord and thickness of the chord.

4 Results

4.1 Numerical analysis

Model 1

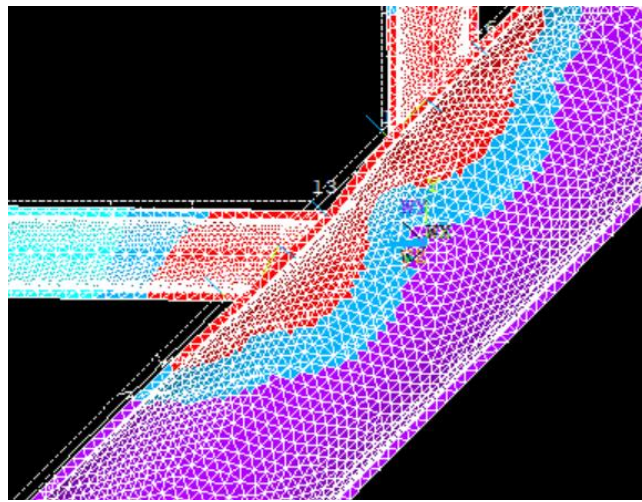


Figure 15: Deformed shape of model 1

Figure 15 presents the deformed shape of fully loaded joint. Point of highest chord indentation is where the compressed brace member makes contact with the chord. Deformation at this point is plotted against applied force in Figure 16.

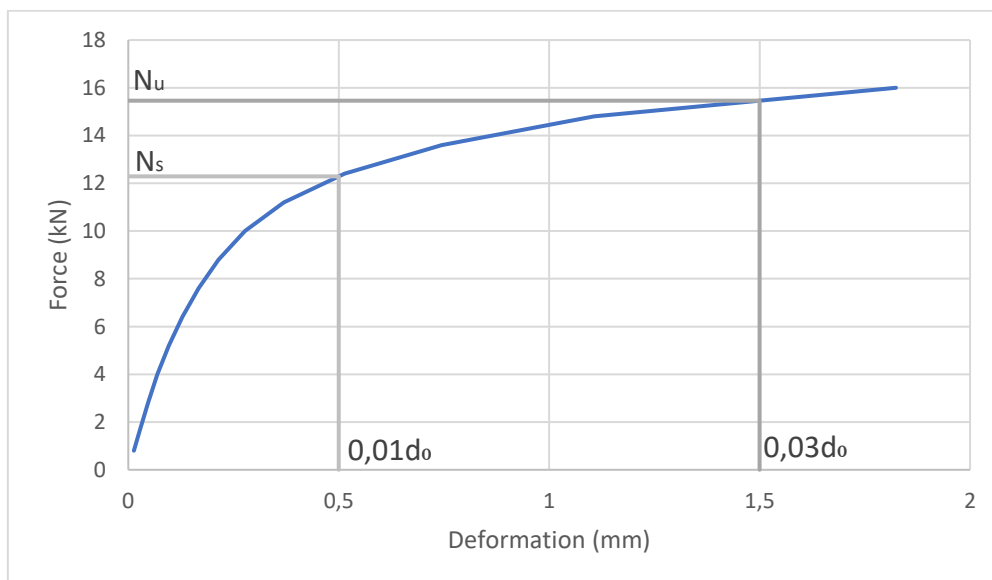


Figure 16: Force-deformation of model 1

From this graph, serviceability limit strength ($N_{s,FEM}$) and ultimate limit strength ($N_{u,FEM}$) are obtained

$$N_{s,FEM} = 12,29 \text{ kN}$$

$$N_{u,FEM} = 15,46 \text{ kN}$$

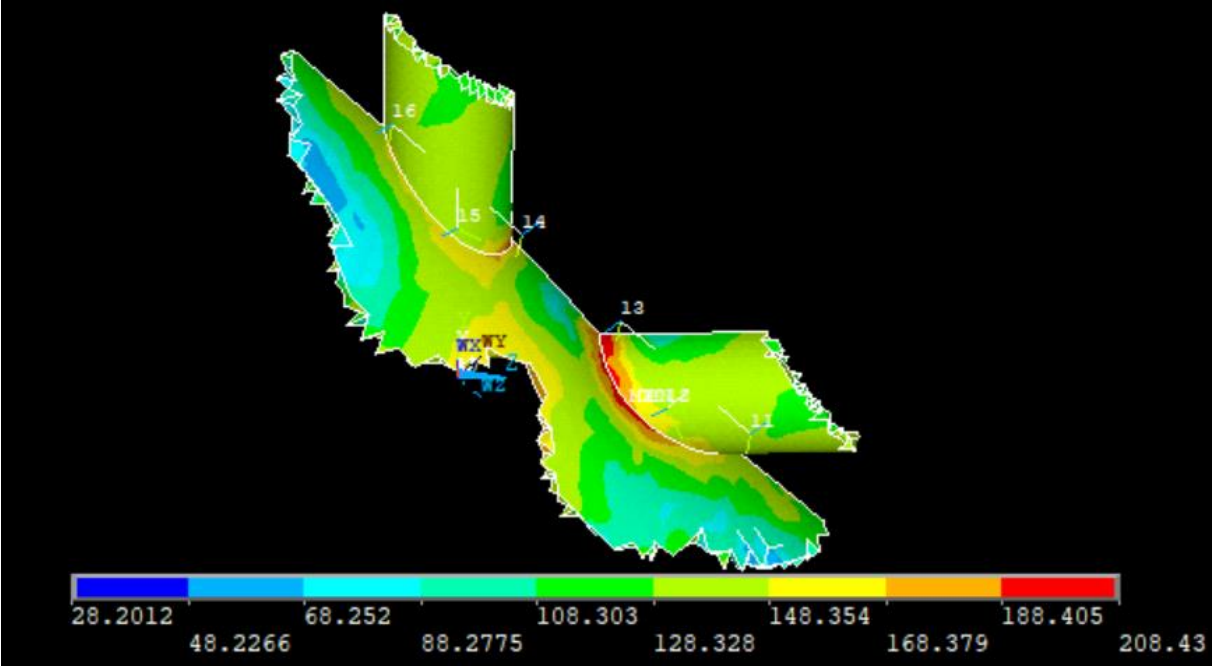


Figure 17: Countur plot of von mises stress in HAZ1 of model 1

Figure 17 depicts the stresses in the heat-affected zone of model 1. Maximum stress is marked with red and is about 208 MPa.

Model 2

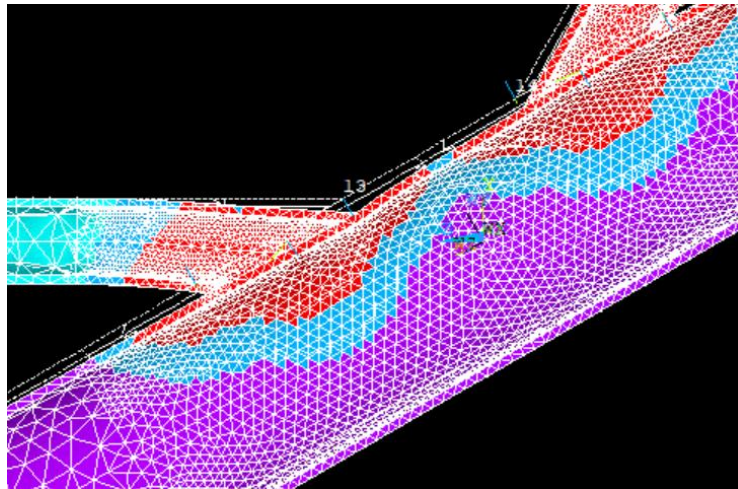


Figure 18: Deformed shape of model 2

In Figure 18, deformed shape of fully loaded joint can be viewed. Point of maximum chord indentation is where the compressed brace member makes contact with the chord. Deformation at this point is plotted against applied force in Figure 19

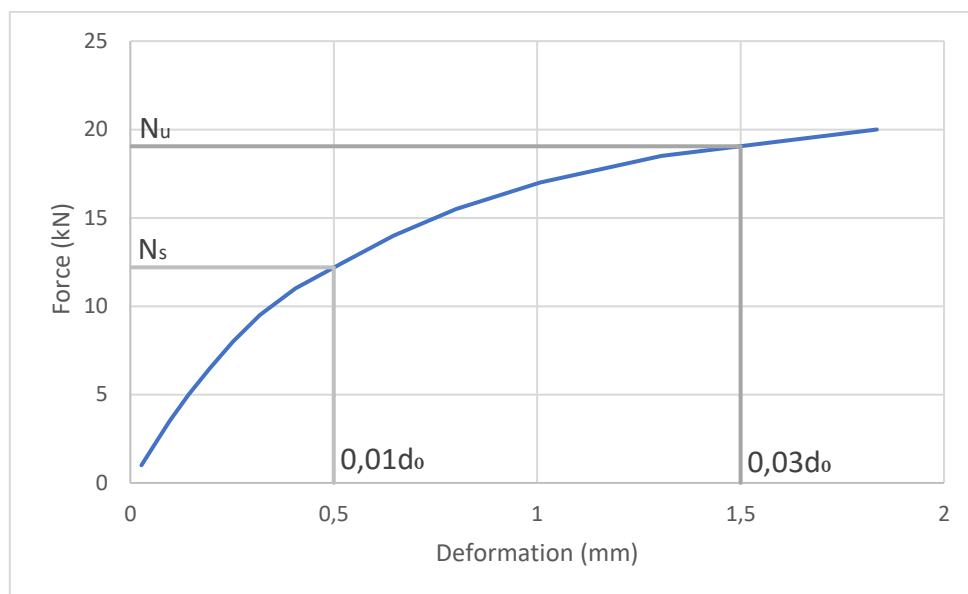


Figure 19: Force-deformation of model 2

From this graph, serviceability limit strength ($N_{s,FEM}$) and ultimate limit strength ($N_{u,FEM}$) are obtained.

$$N_{s,FEM} = 12,19 \text{ kN}$$

$$N_{u,FEM} = 19,05 \text{ kN}$$

Model 3

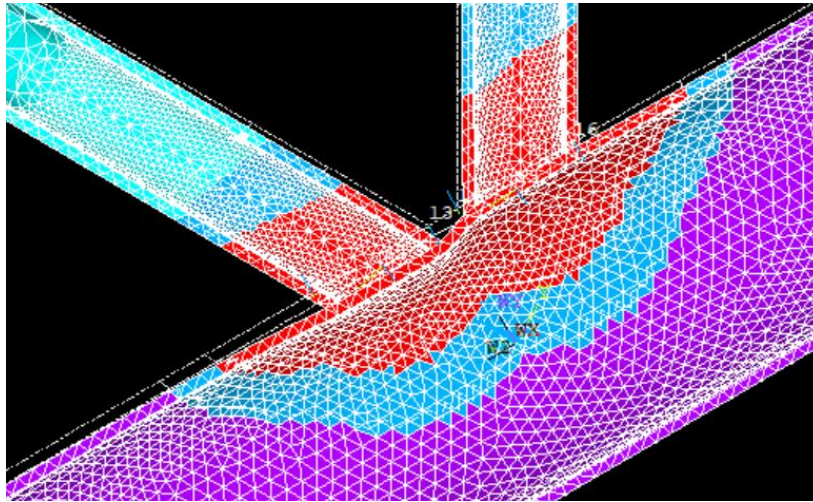


Figure 20: Deformed shape of model 3

Figure 20 shows deformed shape of fully loaded joint. Point of maximum chord indentation is where compressed brace member makes contact with chord. Deformation at this point is plotted together with applied force in Figure 21

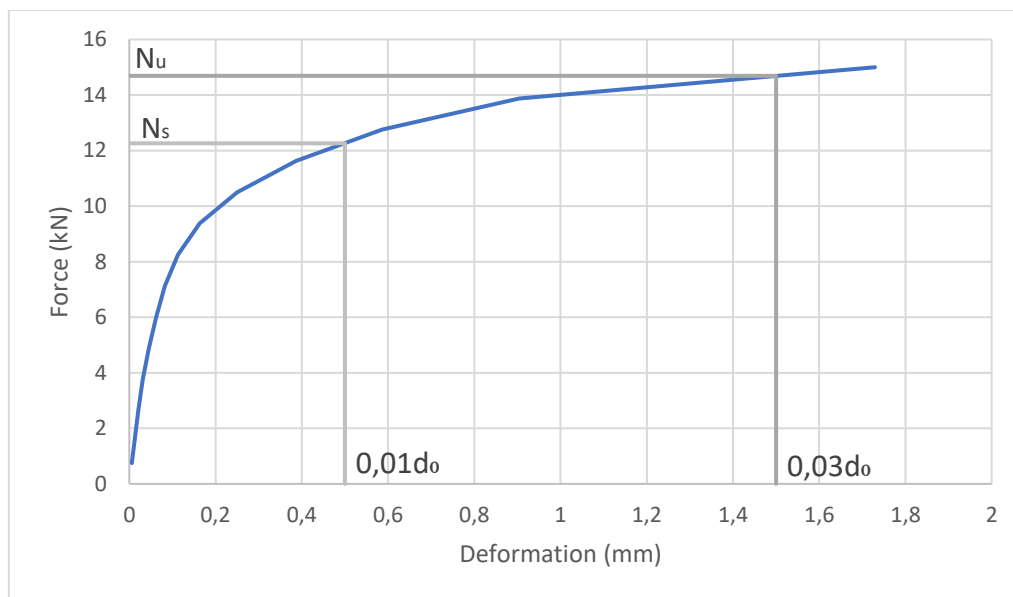


Figure 21: Force-deformation of model 3

From this graph, serviceability limit strength ($N_{s,FEM}$) and ultimate limit strength ($N_{u,FEM}$) are obtained.

$$N_{s,FEM} = 12,26 \text{ kN}$$

$$N_{u,FEM} = 14,69 \text{ kN}$$

Model 4

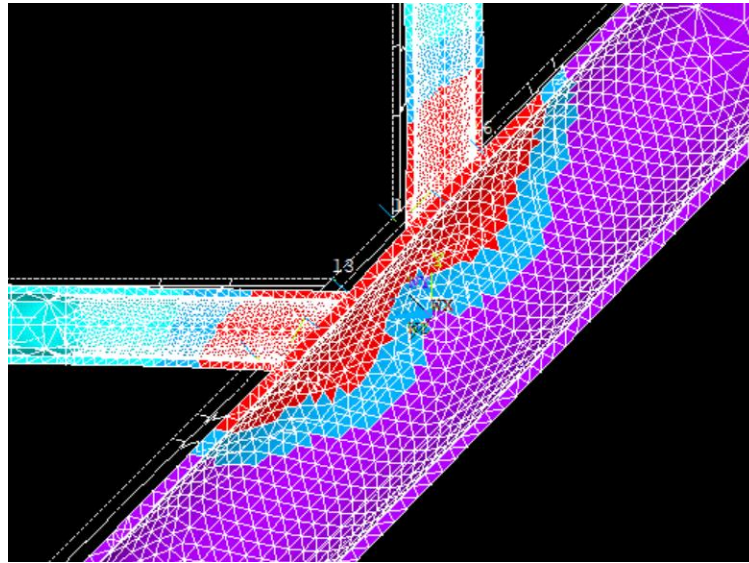


Figure 22: Deformed shape of model 4

Figure 22 shows deformed shape of model 4. From the figure it is hard to immediately see chord indentation at the point where compressed brace meets the chord. This is confirmed by Force-deformation plot in Figure 23. Where it is showed that chord indentation is no more than about 0,5 mm.

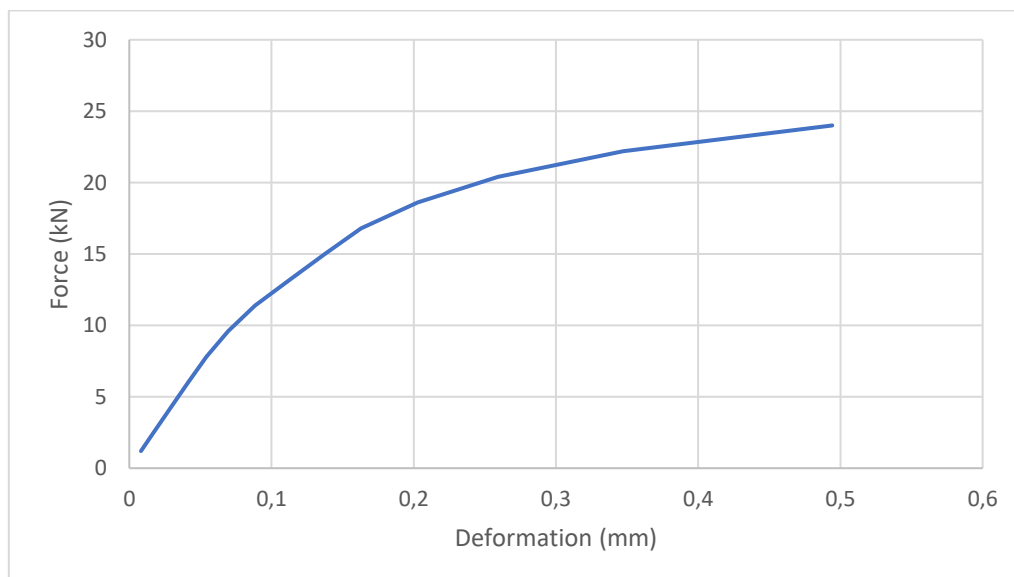


Figure 23: Plot of force-deformation for model 4

At the peak of this graph, right before the joint fails a chord indentation of 0,494 mm and a resistance of 24 kN is obtained. Further loading above 24 kN causes joint to fail.

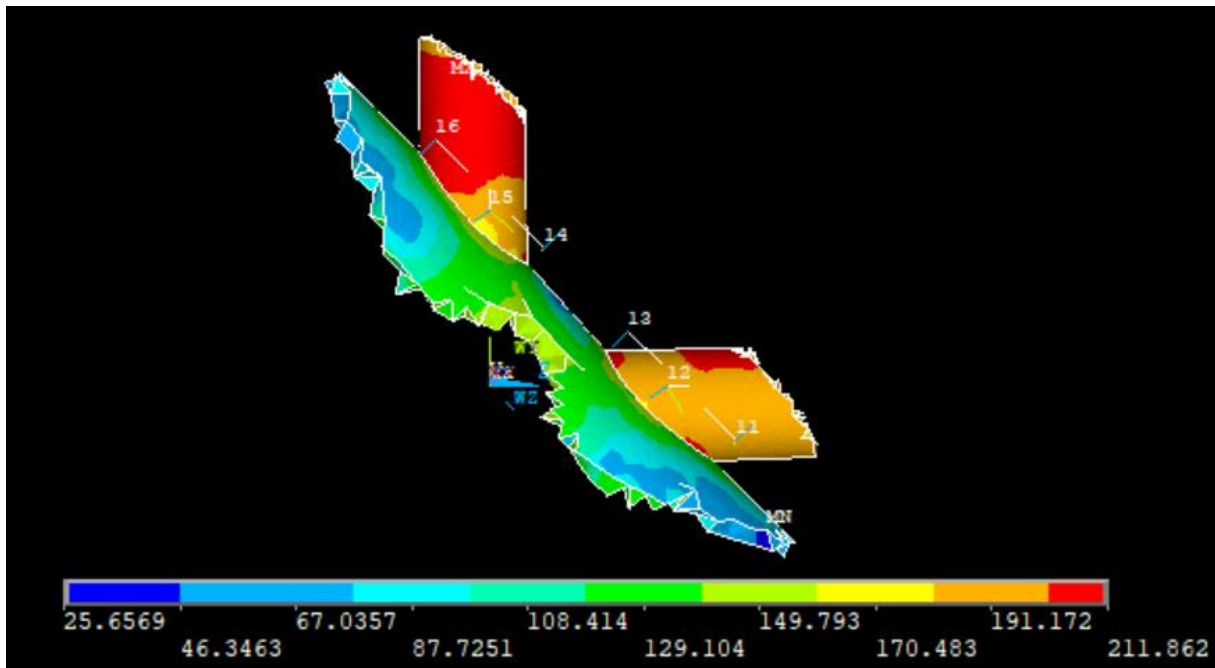


Figure 24: Contour plot of von mises stress in HAZ1 of model 4

Figure 24 shows von mises stresses in heat-affected zone 1 with maximum of 211,862 MPa.

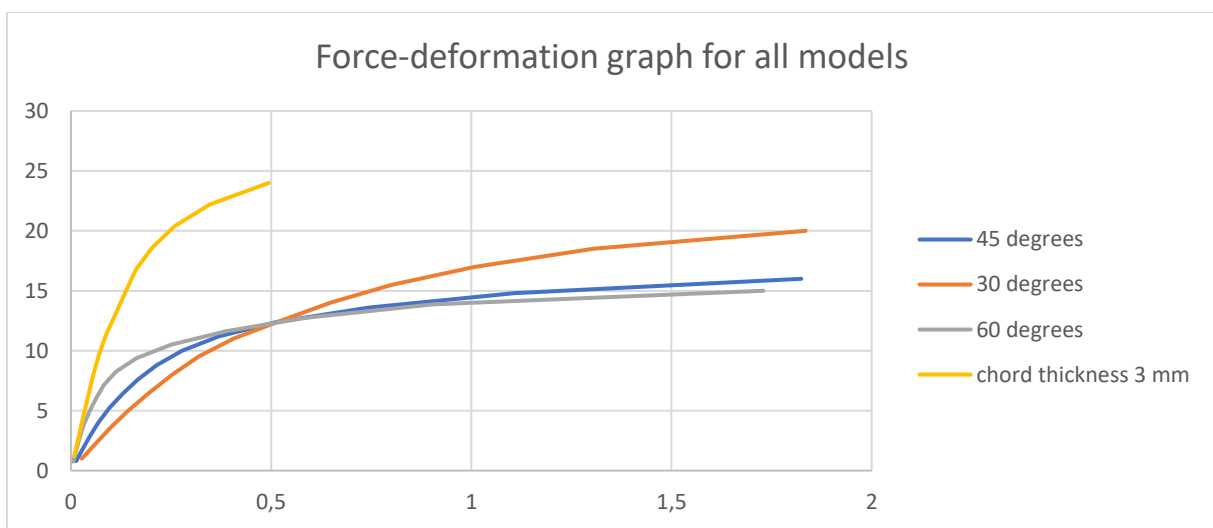


Figure 25: Combined force-deformation graph for all models

Figure 25 depicts all force-deformation graphs for the different models. For the models with 2 mm chord there is a similar resistance at about $0,01d_0$. With load lower than resistance at $0,01d_0$, the joint with the lowest angle experiences more deformation. With loads higher than resistance at $0,01d_0$, the joint with the highest angle experiences more deformation. The joint with chord thickness 3 mm has a lower deformation and the joint resistance at failure is higher.

4.2 Hand calculations

Model 1

Table 18: Results of hand calculations for model 1

Without heat-affected zone softening				With heat-affected zone softening			
Chord plastification		Punching shear		Fully softened		Partially softened	
$N_{1,Rd,cp}$ (kN)	$N_{1,Rd,cp,EN}$ (kN)	$N_{1,Rd,ps}$ (kN)	$N_{1,Rd,ps,EN}$ (kN)	$N_{1,Rd,HAZ}$ (kN)	$N_{1,Rd,HAZ,EN}$ (kN)	$N_{1,Rd,Al}$ (kN)	$N_{1,Rd,Al,EN}$ (kN)
17,16	13,78	38,56	30,96	8,58	6,89	12,56	10,25

Table 18 shows all results for hand calculations done for model 1, both without influence of heat-affected zone and with influence of heat affected zone.

Model 2

Table 19: Results of hand calculations for model 2

Without heat-affected zone softening				With heat-affected zone softening			
Chord plastification		Punching shear		Fully softened		Partially softened	
$N_{1,Rd,cp}$ (kN)	$N_{1,Rd,cp,EN}$ (kN)	$N_{1,Rd,ps}$ (kN)	$N_{1,Rd,ps,EN}$ (kN)	$N_{1,Rd,HAZ}$ (kN)	$N_{1,Rd,HAZ,EN}$ (kN)	$N_{1,Rd,Al}$ (kN)	$N_{1,Rd,Al,EN}$ (kN)
24,16	19,49	67,76	54,41	12,08	9,74	17,68	14,49

Table 19 gives all results for hand calculations done for model 2, both without influence of heat-affected zone and with influence of heat affected zone.

Model 3

Table 20: Results of hand calculations for model 3

Without heat-affected zone softening				With heat-affected zone softening			
Chord plastification		Punching shear		Fully softened		Partially softened	
$N_{1,Rd,cp}$ (kN)	$N_{1,Rd,cp,EN}$ (kN)	$N_{1,Rd,ps}$ (kN)	$N_{1,Rd,ps,EN}$ (kN)	$N_{1,Rd,HAZ}$ (kN)	$N_{1,Rd,HAZ,EN}$ (kN)	$N_{1,Rd,Al}$ (kN)	$N_{1,Rd,Al,EN}$ (kN)
14,04	11,33	28,10	22,56	7,02	5,66	10,28	8,42

Table 20 presents all results for hand calculations done for model 3, both without influence of heat-affected zone and with influence of heat affected zone.

Model 4

Table 21: Results of all hand calculations for model 4

Without heat-affected zone softening				With heat-affected zone softening			
Chord plastification		Punching shear		Fully softened		Partially softened	
$N_{1,Rd,cp}$ (kN)	$N_{1,Rd,cp,EN}$ (kN)	$N_{1,Rd,ps}$ (kN)	$N_{1,Rd,ps,EN}$ (kN)	$N_{1,Rd,HAZ}$ (kN)	$N_{1,Rd,HAZ,EN}$ (kN)	$N_{1,Rd,Al}$ (kN)	$N_{1,Rd,Al,EN}$ (kN)
35,47	28,60	57,84	46,45	17,73	14,30	25,96	21,27

Table 21 gives all results for hand calculations done for model 4, both without influence of heat-affected zone and with influence of heat affected zone.

4.3 Comparison of Numerical results and hand calculations

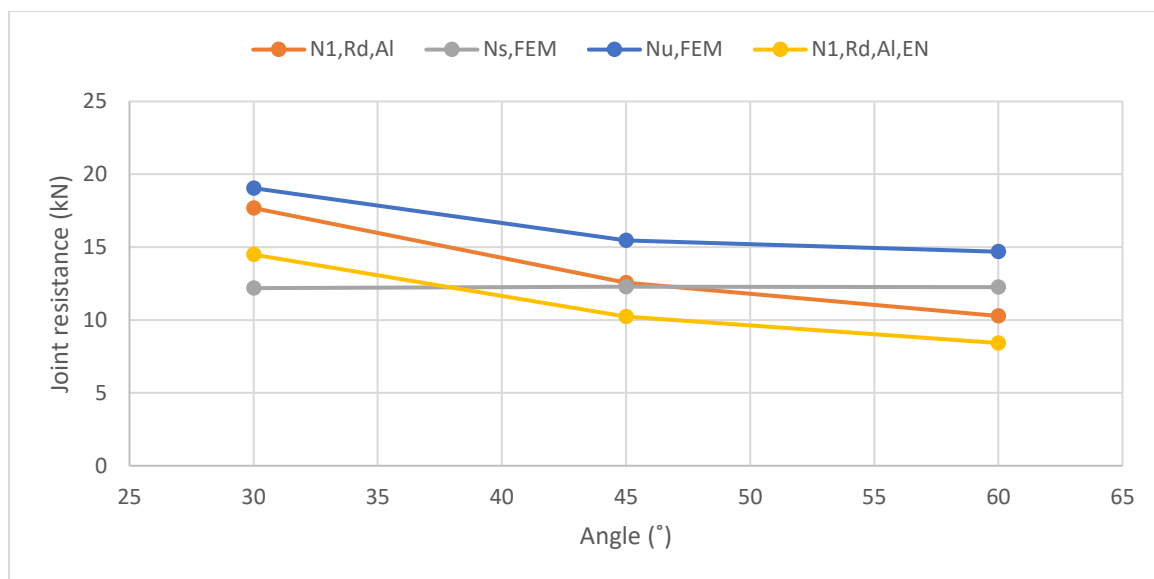


Figure 26: Joint resistances for different angled k-joints

Figure 26 is a graph of the joint resistances as angle of joint varies between 30° and 60°. From the numerical results both N_u and N_s are plotted, these are found in chapter 4.1. Calculated design resistances for partially softened chord cross sections are also plotted in same graph. Design resistances based on both yield strengths from Đuričić et al. (2017) and EN1999-1-1 (2007) are part of the plot.

Table 22: Relation between numerical results and hand calculations

	30°	45°	60°
$\frac{N_u}{N_{1,Rd,Al}}$	1,08	1,23	1,43

Table 22 presents the relationship between ultimate limit strength and calculated design strength for all the connections with brace thickness 2 mm.

Table 23: Relation between different angled connections

Numerical results		Hand calculation results	
$\frac{N_{u,30^\circ}}{N_{u,45^\circ}}$	$\frac{N_{u,45^\circ}}{N_{u,60^\circ}}$	$\frac{N_{1,Rd,Al,30^\circ}}{N_{1,Rd,Al,45^\circ}}$	$\frac{N_{1,Rd,Al,45^\circ}}{N_{1,Rd,Al,60^\circ}}$
1,23	1,05	1,41	1,22

Table 23 gives the relation between resistances of the different angled joints. For the numerical results, the ultimate limit strengths are divided by each other. For the hand calculation results, the partly softened design resistances are divided by each other.

For model 4 the ultimate limit strength is measured at the point where the joint fails since chord indentation is not measured to be higher than 0,494 mm. The relation between numerically obtained strength and hand calculated design resistance against chord indentation is:

$$\frac{N_{u,FEM}}{N_{1,Rd,Al}} = 0,925$$

This shows a higher calculated design resistance than the numerically obtained resistance in the joint.

5 Discussion

5.1 Modelling process

When building a numerical model based on an experimental test it is important to simulate the test in a realistic manner. Nevertheless, some assumptions still need to be made. In our case an important assumption is to consider the braces fixed to the chord without modelling the weld. This has influenced the results. An additional assumption is that the weld failure of the models was not examined. This means that the results preconsider the resistance against tension failure in the weld to be higher than the chord plastification resistance of the aluminium in the joint. This is the conventional way to design a weld and the assumption is therefore realistic. The mesh of the model has been one of the challenges. Since the model is relatively complex it was necessary to divide it in two different parts. The academic version of ANSYS has a limitation of 32000 nodes, so the mesh size in the part around the connection was limited to size level 2 using the smartsize function. An element type with more nodes could have given a better convergence rate and more accurate results, but the node limitation meant that this was not possible. Considering the limited time frame and the lack of the full version of the program, the mesh sizes and convergence of the model have not been able to be more thoroughly investigated.

5.2 Validation of the model

Model 1 in this thesis is constructed to replicate the experimental test by Đuričić et al. (2017) Results from this test were used to validate model 1. Serviceability limit strength and ultimate limit strength against chord plastification failure, according to Lu et al. (1994) explained in chapter 2.4, were obtained from the experimental results and the numerical results. These strengths were compared to each other. For the serviceability limit strength, the comparison gave an accuracy within 0,7 % of the experimental results, which suggests a good correlation between experimental and numerical results. For the ultimate limit strength, the numerical results gave an accuracy within 15 % of the experimental results. However, the measured deformation at failure of the experiment was about 0,75 mm, while the ultimate limit strength

for the numerical results was measured at 1,5 mm deformation. This might be a reason that the results differ so much from each other.

5.3 Interpretation of numerical results of parametric study

5.3.1 Difference in brace angle

The experimental results used a brace angle of 45°, therefore a reference model with this brace angle was created. Additionally, two more brace angles were tested. The lowest recommended brace angle is 30° (EN1993-1-8, 2005), so this value is selected to investigate small brace angles. To investigate angles higher than 45°, a model of brace angle 60° was constructed. The relation between the strengths in the different angle models is graphed in Figure 26. Ultimate limit strength ($N_{u,FEM}$) is significantly different between the models. Table 23 presents the joint resistance in model 2 to be over 20 % higher in comparison to model 1, while model 1 has a higher resistance of 5 % compared to model 3. The cause of the high increase in strength for the model with low brace angle is that most of the load is transferred as axial load in the chord and reduces the chord indentation. While ultimate limit strengths are quite different, the serviceability limit strengths ($N_{s,FEM}$) are practically the same. When load is below serviceability limit strength there is higher deformations in the model with brace angle 30° than for the other models, as presented in Figure 25. From this it can be concluded that lower brace angles give larger deformations in the linear spectrum of the material than higher angles. Since the angle between brace members is lower in model 3, more of the load gets transferred to the tensioned brace member and deformation of the chord will be low until the material reaches its yield strength.

5.3.2 Increased thickness of chord member

It is important to study the stresses in the model when chord member thickness is increased from 2 mm to 3 mm. Figure 24 depicts how the stresses increase in the heat affected zones of the braces, compared to the model of 2 mm chord thickness in Figure 17. This indicates that in model 1 there will be significant chord indentation and eventually this will lead to face failure of the chord. Model 4 shows a different behaviour with less chord indentation and greater total shift of the structure, which gives larger stresses in both braces and eventually the braces will fail in tension before chord face fails. Although the cross-section meets the validity criteria

described in Eurocode 3 part 1-8 (2005), the failure mode differs from expected. The cause of this is the high strength reduction in the heat affected zones for the aluminium, which is not significant when examining steel structures.

5.4 Comparison of hand calculated results and numerical results

For the hand calculations, the joint is considered without softening, with partially softened and fully softened chord. It was decided to use the design strength of the partially softened joint. This strength is calculated over the cross-section which has the largest area of heat affected zone. Since all other cross-sections have a lower area of heat affected zone, this has produced conservative results compared to the actual design resistances. However, it gives more accurate results than the other design resistances where heat softening is not taken into consideration or where fully softened joint is considered. Since the numerical results are based on material strengths from Đuričić et al. (2007), the calculations based on these strengths are the ones with the main focus.

5.4.1 Different brace angles

Figure 26 and Table 23 give highest resistance in model 2 both for the numerical results and the hand calculated results. However, hand calculated results show an increase of 40 % in strength as the angle is changed from 45° to 60°. This is almost twice the increase found in the numerical analysis. The increase in strength is about 20 % when the angle is changed from 60° to 45° which is four times bigger increase than in the numerical analysis. Table 22 shows a good accuracy between numerical and hand calculated results for the model with the lowest brace angle. Strength is reduced by 8 % in comparison to the hand calculated results. For the other models the difference is even bigger, for model 1 there is a reduction of over 20 % and for model 3, a reduction of over 40 %. This should be further investigated to consider if the numerical model needs refining or the hand calculations underestimate the design resistances because of the material.

5.4.2 Different thickness of chord

As stated in chapter 5.3.2 the chord plastification is not the governing failure mode in the model with increased chord thickness. As a consequence of this, the hand calculation resistances are above the numerical limit strengths. These results give a design resistance stated in Table 21 of $N_{1,Rd,Al} = 25,96$ kN, while numerical model fails at about 24 kN. This means that the calculated design resistance of joint cannot be used as a design value when the joint has increased chord thickness. The axial forces of the brace member must also be taken into consideration in the design process.

6 Conclusion

This thesis consists of both numerical and analytical research of a K-joint made from CHS profiles in aluminium alloy EN AW-6082 T6. Although some prior research has been done about this type of joint, it has a limited choice of designing tools available and. The design of aluminium K-joints is still an active research topic.

From the analytical part of the thesis, it is found that a reduction of the angle of the brace member leads to an increase in joint strength. In addition to this, it was found that in the linear spectrum of the stress-strain relation of the material, there will be larger deformations in K-joints with small brace member angles.

The hand calculations done on the basis of EN1993-1-8 (2005) and EN1999-1-1 (2007), give more conservative results than the numerical analysis for the joints with chord thickness of 2 mm. It is important to use a conservative approach when designing structures. However, over 40 % reduction for the joint with brace member of 60° could cause over dimensioning of elements and an economic disadvantage when constructing using aluminium.

The change of chord member thickness influences the model significantly. Even a small change of thickness from 2 mm to 3 mm affects the failure mode that is governing the design resistance. The K-joint designing theory stated in EN1993-1-8 (2005) does not cover the heat affected zones in the brace members. Axial strengths in the braces must also be considered when designing K-joints made from aluminium, since the braces fail from axial forces.

7 Recommended for future work

It might be of interest for the construction industry to investigate the different parameters used in the numerical models and perform experimental tests. This could result in producing more data and to further extent the analytical research in accordance to the calculation methods described in the Eurocodes. Another suggestion is to investigate the validity ranges for the aluminium K-joint for chord plastification failure. This could be used to develop calculation methods for aluminium K-joints, similar to those described for steel K-joints. It would be interesting to investigate N-joints as well and further analyse the complete truss structures, since aluminium CHS-trusses consist of both K-joints and N-joints.

8 References

- ANSYS version 18.2, Academic. ANSYS, Inc, Canonsburg, PA.
- BATHE, K. J. 2006. *Finite Element Procedures*, Prentice Hall.
- CHOO, Y. S., QIAN, X. D., LIEW, J. Y. R. & WARDENIER, J. 2003. Static strength of thick-walled CHS X-joints—Part I. New approach in strength definition. *Journal of Constructional Steel Research*, 59, 1201-1228.
- ĐURIČIĆ, Đ., ALEKSIĆ, S., ŠĆEPANOVIĆ, B. & LUČIĆ, D. 2017. Experimental, theoretical and numerical analysis of K-joint made of CHS aluminium profiles. *Thin-Walled Structures*, 119, 58-71.
- EN573-3 2013. Aluminium and aluminium alloys, chemical composition and form of wrought products. *Part 3: Chemical composition and form of products*. Brussels: CEN.
- EN755-2 2016. Aluminium and aluminium alloys, Extruded rod/bar, tube and profiles. *Part 2: Mechanical properties*. Brussels: CEN.
- EN1993-1-8 2005. Eurocode 3: Design of steel structures. *Part 1-8: Design of joints*. Brussels: CEN.
- EN1999-1-1 2007. Eurocode 9: Design of aluminium structures. *Part 1-1: General structural rules*. Brussels: CEN.
- EN-ISO-6507-1 2005. Metallic materials, Vickers hardness test. *Part 1: Test method*. Brussels: CEN.
- GERE, J. M. 2004. *Mechanics of materials*, Belmont, CA, USA, Thomson Learning, Inc.
- LU, L. H., WINKEL, G. D. D., YU, Y. & WARDENER, J. 1994. Deformation limit for the ultimate strength of hollow section joints. *Proceedings of Sixth International Symposium on Tubular Structures*.
- MAC DONALD, B. 2007. *Practical Stress Analysis with Finite Elements*, Dublin, Ireland, Glasnevin Publishing.
- MATUSIAK, M. 1999. *Strength and ductility of welded structures in aluminum alloys*. Doctor thesis, Norwegian University of science and technology.
- MAZZOLANI, F. M. 2012. 3D aluminium structures. *Thin-Walled Structures*, 61, 258-266.
- MÜLLER, U. 2011. Introduction to structural aluminium design. Whittles Publishing.
- VAN HOVE, B. W. E. M. & SOETENS, F. 2016. Numerical/experimental research on welded joints in aluminium truss girders. *Aluminium Constructions : Sustainability, Durability and Structural Advantages : Selected, Peer-Reviewed Papers from the 13th International Aluminium Conference - INALCO 2016, September 21-23, 2016, Napels, Italy*.
- WANG, T. 2006. *Modelling of Welded Thin-Walled Aluminium Structures*. Doctoral thesis, Norwegian University of Science and Technology.

- WANG, Y., FAN, F. & LIN, S. 2015. Experimental investigation on the stability of aluminium alloy 6082 circular tubes in axial compression. *Thin-Walled Structures*, 89, 54-66.
- WARDENIER, J. 2001. Hollow sections in structural applications. S.I.: CIDECT, Comité international pour le développement et l'étude de la construction tubulaire.
- WARDENIER, J., KUROBANE, Y., PACKER, J. A., VAN DER VEGTE, A. & ZHAO, X. L. 2008. *Design Guide for circular hollow section (CHS) joints under predominantly static loading*, Zoetermeer, Netherlands.

Annex A

Measured deformations in numerical model

The measuring of deformation was done in three points. Point of maximum chord indentation and upward and downward measuring points to calculate total shift of the structure in point of maximum chord indentation. The points are shown in Figure A 1.

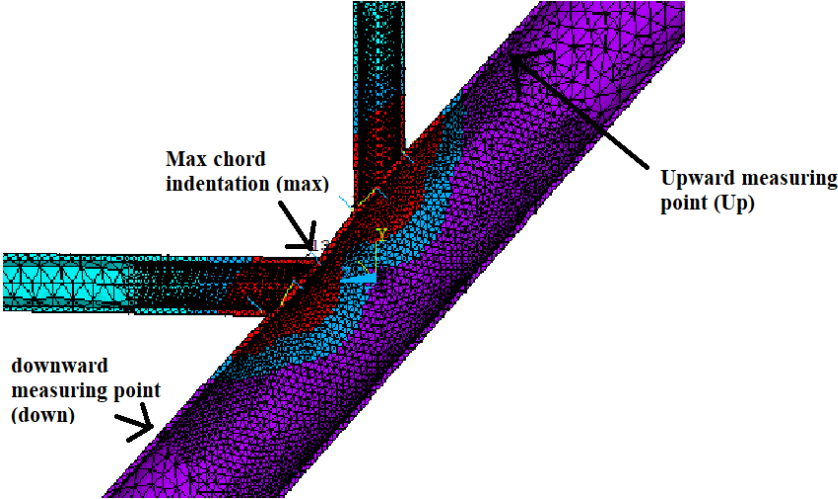


Figure A 1: Measured points in the numerical models

Table A 1 gives total deformation in point of maximum chord indentation (D_{max}), deformation in downward measuring point (D_{down}), deformation in upward measuring point (D_{up}), shift of structure in point of maximum chord indentation ($Shift_{max}$) and chord indentation in point of maximum chord indentation ($D_{max,c-ind}$). These deformations are given in all timesteps of the simulation.

Table A 1: Measured deformations in model 1

time	D_max (mm)	D_down (mm)	D_up (mm)	Shift_max (mm)	D_max,c-ind (mm)
0,050	0,09112089	0,09557962	0,06019791	0,07788877	0,01323212
0,100	0,18233851	0,19130138	0,12037022	0,1558358	0,02650272
0,175	0,31945387	0,33519548	0,21056763	0,27288156	0,04657232
0,250	0,45941859	0,48066644	0,30065756	0,390662	0,06875659
0,325	0,60761332	0,63123847	0,3916615	0,51144998	0,09616334
0,400	0,76610494	0,79040184	0,48468846	0,63754515	0,12855979
0,475	0,93659334	0,95930136	0,57977099	0,76953618	0,16705716
0,550	1,12261616	1,13807069	0,67901272	0,9085417	0,21407446
0,625	1,33806523	1,33544257	0,78605596	1,06074927	0,27731597
0,700	1,59471954	1,55080114	0,90021835	1,22550974	0,3692098
0,775	1,92855596	1,79982435	1,03005942	1,41494188	0,51361408
0,850	2,38440649	2,09766055	1,18224789	1,63995422	0,74445227
0,925	3,018455	2,45684251	1,36534683	1,91109467	1,10736033
1,000	4,06975308	2,89746903	1,59392687	2,24569795	1,82405513

The same points are used for the other models. Table A 2, Table A 3 and Table A 4 show deformations in the other models.

Table A 2: Measured deformations for model 2

time	D_max (mm)	D_down (mm)	D_up (mm)	Shift_max (mm)	D_max,c-ind (mm)
0,050	0,09031098	0,04398118	0,08189504	0,06293811	0,02737287
0,100	0,1808276	0,08805746	0,1639247	0,12599108	0,05483652
0,175	0,31759709	0,1544941	0,28724623	0,22087016	0,09672692
0,250	0,4603849	0,22308995	0,41175984	0,3174249	0,14296001
0,325	0,61915518	0,30586439	0,54082202	0,4233432	0,19581198
0,400	0,79235734	0,40624224	0,67388425	0,54006324	0,25229409
0,475	0,98158981	0,51305356	0,81274224	0,6628979	0,31869191
0,550	1,20559645	0,63263354	0,96642923	0,79953138	0,40606507
0,625	1,49151453	0,79564514	1,13852233	0,96708374	0,52443079
0,700	1,87805867	1,1217263	1,33958448	1,23065539	0,64740328
0,775	2,33717625	1,51287419	1,56015774	1,53651597	0,80066028
0,850	2,86965985	1,92751111	1,79618732	1,86184922	1,00781063
0,925	3,51219825	2,3585504	2,05399992	2,20627516	1,30592309
1,000	4,43512654	2,82095662	2,37966787	2,60031224	1,8348143

Table A 3: Measured deformations for model 3

time	D_max (mm)	D_down (mm)	D_up (mm)	Shift_max (mm)	D_max,c- ind (mm)
0,050	0,05786381	0,06207318	0,04194312	0,05200815	0,00585566
0,100	0,11573591	0,12415747	0,08387295	0,10401521	0,01172071
0,175	0,20257155	0,21731642	0,14673987	0,18202815	0,02054341
0,250	0,29195548	0,31220705	0,20976163	0,26098434	0,03097115
0,325	0,38824211	0,41194086	0,27421779	0,34307932	0,04516278
0,400	0,49083891	0,51617159	0,34076811	0,42846985	0,06236906
0,475	0,60019158	0,62623578	0,40911082	0,5176733	0,08251829
0,550	0,72684294	0,74746654	0,4804741	0,61397032	0,11287262
0,625	0,88897002	0,89127539	0,55965852	0,72546696	0,16350306
0,700	1,11204623	1,06910319	0,65450706	0,86180513	0,2502411
0,775	1,41418869	1,28395107	0,7711033	1,02752719	0,38666151
0,850	1,80773823	1,53216304	0,9108119	1,22148747	0,58625076
0,925	2,34907689	1,81467581	1,07520264	1,44493923	0,90413767
1,000	3,45488448	2,17328982	1,27788987	1,72558985	1,72929463

Table A 4: Measured deformations for model 4

time	D_max (mm)	D_down (mm)	D_up (mm)	Shift_max (mm)	D_max,c- ind (mm)
0,050	0,11251667	0,1270627	0,08156774	0,10431522	0,00820145
0,100	0,22518805	0,25444106	0,16315089	0,20879598	0,01639208
0,175	0,39454154	0,4461363	0,28555093	0,36584361	0,02869793
0,250	0,56522722	0,63955758	0,40797091	0,52376425	0,04146297
0,325	0,74125721	0,84295967	0,53112417	0,68704192	0,05421529
0,400	0,93217887	1,06300352	0,66241975	0,86271164	0,06946723
0,475	1,13638353	1,2956855	0,80003758	1,04786154	0,08852199
0,550	1,35375735	1,53724378	0,94422514	1,24073446	0,11302289
0,625	1,58333795	1,79992617	1,09170428	1,44581523	0,13752272
0,700	1,85995954	2,12281941	1,27133698	1,6970782	0,16288134
0,775	2,45597277	2,81352131	1,69308941	2,25330536	0,20266741
0,850	3,21401245	3,68125447	2,22807933	2,9546669	0,25934555
0,925	4,16253256	4,74432588	2,88633917	3,81533252	0,34720004
1,000	5,45519447	6,14868237	3,77317835	4,96093036	0,4942641

Annex B

Vickers hardness testing method

Vickers hardness test is performed according to EN ISO 6507-1. A diamond indenter formed as a pyramid with a specified angle, $\alpha = 136^\circ$, at the tip is forced into the specimen surface. This makes a square mark in the test piece. The diagonals (d_1, d_2) are measured and the arithmetic mean of these (d) are calculated (EN-ISO-6507-1, 2005). The method above is presented in Figure B 1 and Figure B 2.

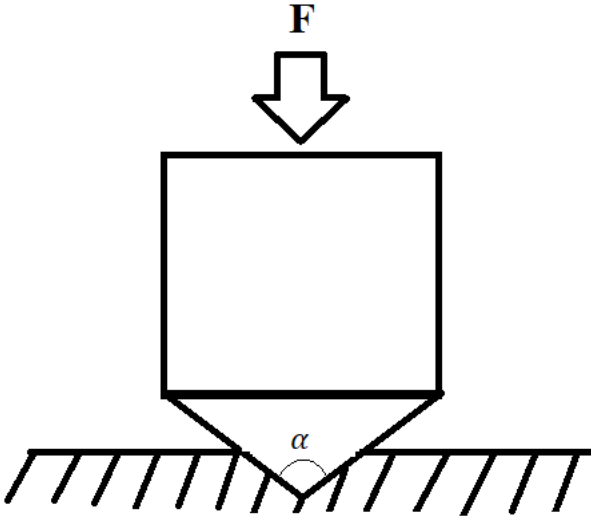


Figure B 1: Diamond indenter forced into surface of test specimen

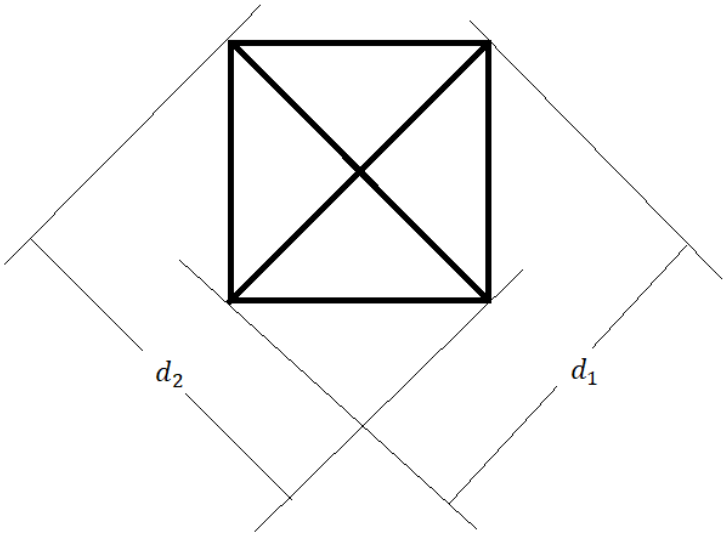


Figure B 2: Square mark in test specimen with two diagonals

To calculate Vickers hardness (HV) equation underneath is used.

$$HV = 0,1891 \frac{F}{d^2} \quad (B1)$$

Where:

F is the test force, in newtons (N)

d is the arithmetic mean, in millimetres (mm)

Annex C

Strength reduction coefficient for heat affected zone

To calculate strength reduction coefficient in the heat affected zone of the chord, the cross-section is assumed as in Figure C 1.

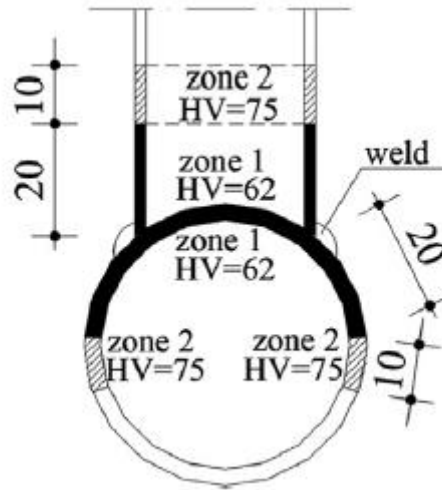


Figure C 1: Cross-section of chord with two heat affected zones (Đuričić et al., 2017)

Distance inside the brace member is set to 20 and average hardness (HV_{av}) needs to be calculated:

$$HV_{av} = \frac{l_{HAZ1} * HV_{HAZ1} + l_{HAZ2} * HV_{HAZ2}}{l_{HAZ1} + l_{HAZ2}} \quad (C1)$$

Where:

l_{HAZ1} is length of HAZ1 (mm)

HV_{HAZ1} is Vickers hardness of HAZ1

l_{HAZ2} is length of HAZ2 (mm)

HV_{HAZ2} is Vickers hardness of HAZ2

$$HV_{av} = \frac{60 * 62 + 20 * 75}{60 + 20} = 65,25$$

Then equation (3) is applied to find the yield strength

$$f_{0,HAZ} = 3HV_{av} - 48,1 = 147,65 \text{ MPa}$$

Then equation (22) is applied to find strength reduction factor

$$\rho_{0,haz} = \frac{f_{0,haz}}{f_0} = \frac{147,65 \text{ MPa}}{309,34 \text{ MPa}} = 0,477$$



Norges miljø- og biovitenskapelige universitet
Noregs miljø- og biovitenskapelige universitet
Norwegian University of Life Sciences

Postboks 5003
NO-1432 Ås
Norway